



Deformation patterns of upper Quaternary strata and their relation to active tectonics, Po Basin, Italy

ALESSANDRO AMOROSI* , LUIGI BRUNO† , BRUNO CAMPO*,
BIANCA COSTAGLI*, WAN HONG‡, VINCENZO PICOTTI§ and
STEFANO CLAUDIO VAIANI*

*Department of Biological, Geological and Environmental Sciences, University of Bologna, Via
Zamboni 67, Bologna 40126, Italy (E-mail: alessandro.amorosi@unibo.it)

†Department of Chemical and Geological Sciences, University of Modena and Reggio Emilia, Via
Campi 103, Modena 41125, Italy

‡KIGAM Korea Institute of Geoscience and Mineral Resources, 92 Gwahangro, Yuseong-gu, Daejeon,
South Korea

§Department of Earth Sciences, ETH, Sonneggstrasse 5, Zurich 8092, Switzerland

Associate Editor – Adam McArthur

ABSTRACT

Despite increased application of subsurface datasets below the limits of seismic resolution, reconstructing near-surface deformation of shallow key stratigraphic markers beneath modern alluvial and coastal plains through sediment core analysis has received little attention. Highly resolved stratigraphy of Upper Pleistocene to Holocene (Marine Isotope Stage 5e to Marine Isotope Stage 1) alluvial, deltaic and coastal depositional systems across the southern Po Plain, down to 150 m depth, provides an unambiguous documentation on the deformation of previously flat-lying strata that goes back in time beyond the limits of morphological, historical and palaeoseismic records. Five prominent key horizons, accurately selected on the basis of their sedimentological characteristics and typified for their fossil content, were used as highly effective stratigraphic markers (M1 to M5) that can be tracked for tens of kilometres across the basin. A facies-controlled approach tied to a robust chronology (102 radiocarbon dates) reveals considerable deformation of laterally extensive nearshore (M1), continental (M2 and M3) and lagoon (M4 and M5) marker beds originally deposited in a horizontal position (M1, M4 and M5). The areas where antiformal geometries are best observed are remarkably coincident with the axes of buried ramp anticlines, across which new seismic images reveal substantially warped stratal geometries of Lower Pleistocene strata. The striking spatial coincidence of fold crests with the epicentres of historic and instrumental seismicity suggests that deformation of marker beds M1 to M5 might reflect, in part at least, syntectonically generated relief and, thus, active tectonism. Precise identification and lateral tracing of chronologically constrained stratigraphic markers in the ^{14}C time window through combined sedimentological and palaeoecological data may delineate late Quaternary subsurface stratigraphic architecture at an unprecedented level of detail, outlining cryptic stratal geometries at the sub-seismic scale. This approach is highly reproducible in tectonically active Quaternary depositional systems and can help to assess patterns of active deformation in the subsurface of modern alluvial and coastal plains worldwide.

Keywords Holocene, near-surface deformation, Po Plain, Quaternary, sediment core analysis, stratigraphic marker.

INTRODUCTION

Conventional seismic analysis in onshore regions generally provides insufficient resolution into the identification of thrust-related deformation of upper Quaternary strata. In such areas, geomorphic and palaeoseismic data of Quaternary age are routinely used for detecting active tectonics. Geomorphic data include uplifted fluvial or marine terraces, changes in stream gradients, vegetation lineaments, topographic scarps and aligned drainages (e.g. Azor *et al.*, 2002; Keller & Pinter, 2002; Picotti & Pazzaglia, 2008; Rossetti *et al.*, 2014; Whitney & Hengesh, 2015; Matsu'ura & Sugaya, 2017). Palaeoseismic investigations comprise excavation of trenches and surficial coring surveys (e.g. Barka *et al.*, 2002; Prentice *et al.*, 2010; Audemard & Michetti, 2011). However, in modern alluvial and coastal plains developed on top of actively subsiding basins, tectonics can have no significant or persistent geomorphic expression. Far from the basin margins, in particular, tectonically-generated accommodation is systematically counterbalanced by depositional filling, and the record of past seismic events is no longer prominent in the resulting flat morphology. On the other hand, shallow coring or trenching datasets are spatially limited and provide highly fragmentary point data that are typically focused on very short temporal scales that can be poorly representative of the past seismic activity. In particular, large earthquakes with recurrence intervals of several centuries to a few millennia can be missed by the use of temporally short datasets. As a consequence, geological records on centennial to millennial temporal scales and high-resolution near-surface stratigraphic studies are crucial to understand the occurrence of large, but infrequent, seismic events (Begg *et al.*, 1993; Sinha *et al.*, 2005; Ishiyama *et al.*, 2007, 2013; Dura *et al.*, 2016).

The Po Plain (northern Italy) has been the object of intensive geophysical surveys and drillings by oil companies, aimed at an improved characterization of the petroleum systems in the area (Pieri & Groppi, 1981; Ghielmi *et al.*, 2010, 2013; Amadori *et al.*, 2019). Previous stratigraphic studies have focused largely on the deformation of the Pliocene to Middle Pleistocene syntectonic basin fill and prominent basin-scale unconformities have been tracked in the subsurface (Regione Emilia-Romagna & ENI-AGIP, 1998; Regione Lombardia & ENI-Divisione Agip, 2002; Muttoni *et al.*, 2003; Ghielmi *et al.*, 2010, 2013;

Garzanti *et al.*, 2011; Bresciani & Perotti, 2014; Amadori *et al.*, 2019). In contrast, deformation of Upper Pleistocene–Holocene deposits over the past 125 kyr has received very little study.

The Po Plain is historically a region with rare earthquakes greater than magnitude 5. In 2012, it experienced two M_w ca 6.0 damaging earthquakes close to the village of Mirandola (Fig. 1A). Coseismic surface ruptures in the central sector of the buried Ferrara arc resulted in ground fractures associated with widespread soil liquefaction phenomena and a 15 to 20 cm anticlinal crest growth (Caputo *et al.*, 2015; Caranante *et al.*, 2015). This fact raised the issue of seismic hazard assessment in the area. Following the 2012 Po Plain earthquakes, several palaeoseismic and historical earthquake studies were undertaken, and a few studies addressed some aspects of the possible use of combined sedimentological and stratigraphic criteria to assess the deformation of Quaternary strata. These studies, however, suffered from a lack of palaeotopographic accuracy, because they focused on palaeosurfaces that were far from being horizontal at the time of formation: for example, palaeosols (Amorosi *et al.*, 2017b) and fluvial channel-belts (Stefani *et al.*, 2018).

Upper Pleistocene–Holocene sedimentary successions in tectonically active regions are key to understanding syndepositional tectonics, because they provide information on a millennial timescale. Few researchers only, however, have used the spatial distribution of sedimentary facies to depict the deformation of near-surface, upper Quaternary strata (Ishiyama *et al.*, 2007; Tamura *et al.*, 2010; Niwa *et al.*, 2019; Niwa & Sugai, 2020). This paper explores the deformation of targeted stratigraphic markers that approximate palaeohorizontal surfaces through accurate facies analysis of a relatively shallow (<150 m), Upper Pleistocene–Holocene sedimentary succession. The south-eastern Po Plain serves as a very useful location for high-resolution Quaternary records, as it has received intensive study, and a comprehensive sequence stratigraphic, sedimentological and palaeontological framework, chronologically constrained by over 200 radiocarbon dates, is available (Campo *et al.*, 2017; Amorosi *et al.*, 2017a,b; Bruno *et al.*, 2017b). The approach taken here involves the high-resolution study of drill cores of Late Pleistocene–Holocene age from the shallow subsurface, coupled with the seismic stratigraphic analysis of the basin fill.

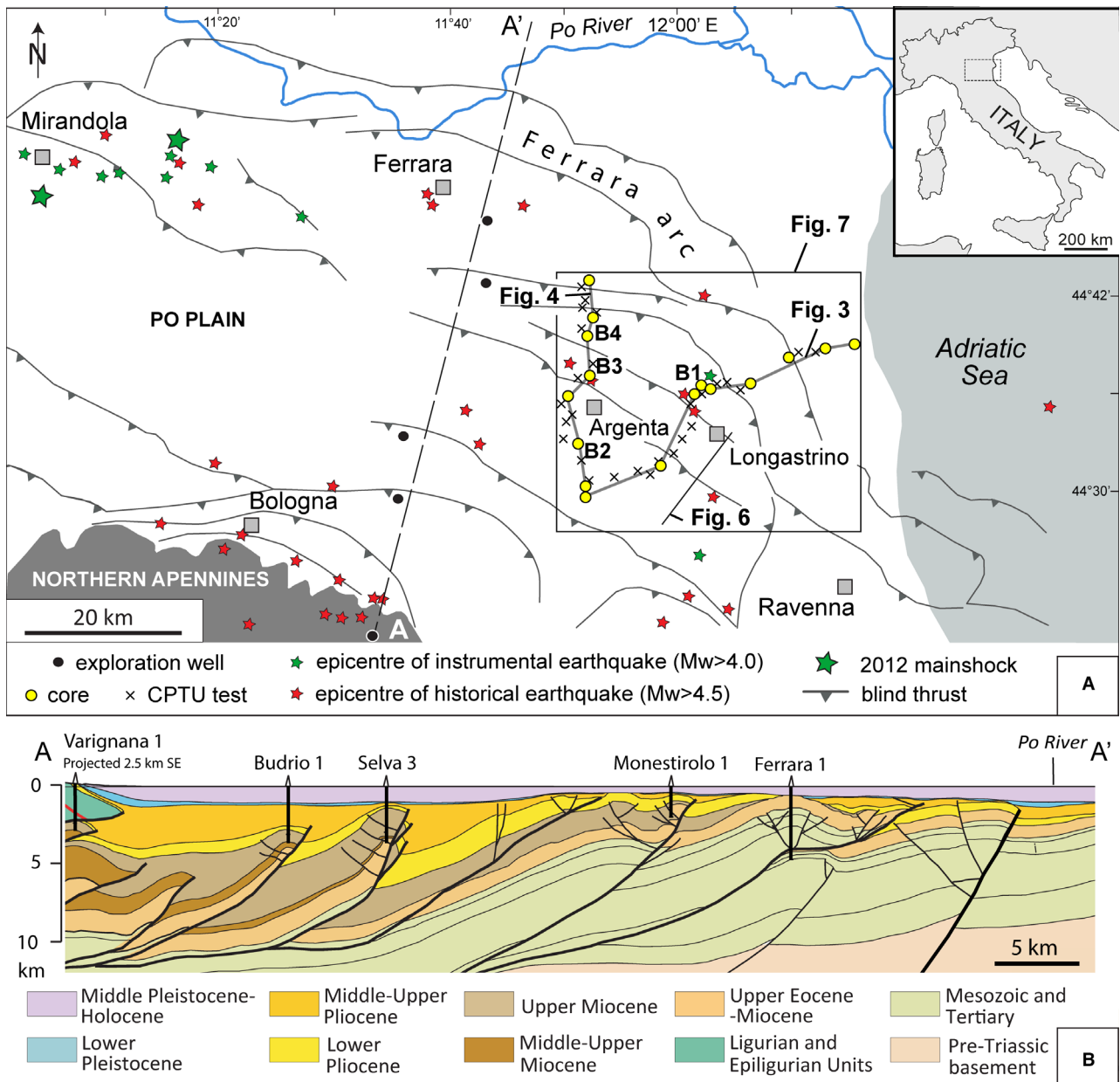


Fig. 1. (A) Study area, structural setting, with location of the Ferrara arc and minor thrust fronts, and the earthquake catalogue, with spatial distribution of historical and instrumental earthquakes $>M_w$ 4.5 and $>M_w$ 4.0, respectively. Section traces of Figs 4, 5 and 7 are also shown. B1 to B4: cores of Fig. 2. (B) Schematic profile showing the major fold-and-thrust belt structures buried beneath the Po Plain (modified after Picotti & Pazzaglia, 2008; see dashed line in Fig. 1A, for location).

Previous stratigraphic work from the Po River system has focused on reconstructing the sequence-stratigraphic architecture of the upper Quaternary succession, on a basin scale (Campo *et al.*, 2017, 2020a; Amorosi *et al.*, 2017a, 2020; Bruno *et al.*, 2017a,b). Through a high-resolution stratigraphic framework of shallow buried depositional systems, chronologically constrained by 102 radiocarbon dates, this paper shows how

combined sedimentological and palaeoecological examination of alluvial, deltaic and coastal core deposits can be used for the identification and lateral tracing in the subsurface of prominent key horizons with distinctive facies characteristics. Based on the geometry of such marker beds and its comparison with the location of major tectonic structures and historical/instrumental records of seismic activity, the aim of this paper

is to assess patterns of active deformation on millennial timescales, i.e. below the resolution of conventional seismic stratigraphy and beyond the short temporal scales intrinsic to geomorphic and palaeoseismic datasets.

GEOLOGICAL SETTING

The northern Apennines ‘thrust and fold’ belt developed since the Oligocene in the context of the collision between the European plate and the Adria plate. The development of the Apennines foredeep, in particular, has been related to the eastward rollback of the subducting Adria plate (Malinverno & Ryan, 1986; Royden *et al.*, 1987; Doglioni, 1993). The northern Apennines foreland basin evolved through a series of successive regional tectonic phases that led to the progressive outward (north-east) migration of the thrust and fold belt and related foredeeps (Ricci Lucchi, 1986). The Po Plain–Adriatic foredeep, bounded by the outermost thrust-propagation folds of the northern Apennines at its inner margin, and by the Adriatic foreland ramp at the outer margin, was affected by active synsedimentary compressional tectonics since the Late Miocene (Ghielmi *et al.*, 2013). The Quaternary geodynamic evolution and the tectonic processes active along the northern Apennines thrust fronts and in the adjacent Po–Adriatic foredeep domains have been analysed and discussed at length by several authors (e.g. Picotti & Pazzaglia, 2008; Fantoni & Franciosi, 2010; Bresciani & Perotti, 2014; Gunderson *et al.*, 2018).

The geometry of the northern Apennines accretionary prism consists of three main arcuate thrust systems (Monferrato, Emilia and Ferrara–Romagna–Adriatic arcs in Amadori *et al.*, 2019). The buried thrusts and related fault-propagation folds beneath the modern Po Plain have been investigated through interpretation of a dense network of seismic lines and well logs (Pieri & Groppi, 1981; Picotti *et al.*, 2007; Picotti & Pazzaglia, 2008; Toscani *et al.*, 2009; Fantoni & Franciosi, 2010; Ghielmi *et al.*, 2013; Martelli *et al.*, 2017; Livani *et al.*, 2018; Amadori *et al.*, 2019). Anticline structures are associated with ramp overthrusts and are separated by large synclines (Fig. 1B) that record much larger subsidence rates (Carminati *et al.*, 2003; Ghielmi *et al.*, 2010; Martelli *et al.*, 2017). The Ferrara arc represents one of the most external structures of the northern Apennines (Fig. 1A): it has been tectonically active since the Early Pliocene

to present times (Scrocca *et al.*, 2007; Toscani *et al.*, 2009; Boccaletti *et al.*, 2011; Maesano *et al.*, 2015; DISS Working Group, 2018). Distinct thrust systems belong to the Ferrara arc (Fig. 1A and B): the Mirandola structure, at the western edge of the Ferrara arc (Fig. 1A), includes active seismogenic faults (Bonini *et al.*, 2014; Govoni *et al.*, 2014; Martelli *et al.*, 2017). The Longastrino–Argenta thrust system, to the east (Fig. 1A), received comparatively little attention (Toscani *et al.*, 2009; Maesano *et al.*, 2015), although this area was hit by a devastating earthquake in 1624 (Livio *et al.*, 2014).

The major architectural components of the Pliocene–Quaternary Po Basin fill stack to form a two-fold, cyclic hierarchy of: (i) third-order depositional sequences, separated at the basin margin by tectonically formed angular unconformities (Regione Emilia-Romagna & ENI-AGIP, 1998; Regione Lombardia & ENI-Divisione Agip, 2002; Amadori *et al.*, 2019); and (ii) fourth-order (100 kyr), transgressive–regressive (T–R) sequences controlled by glacio-eustatic fluctuations (Amorosi *et al.*, 2004, 2008). The younger successions display progressively lower deformation than older deposits. Distinctive cyclic alternations of coastal and alluvial facies are the most prominent feature of T–R sequences. The youngest two transgressive surfaces, recording the Last Interglacial and Holocene marine incursions, respectively, are best recognized beneath the modern coastal plain (Amorosi *et al.*, 2004). The uppermost two T–R sequences, which cover the MIS 5 to MIS 1 stratigraphic interval, are the focus of this study.

METHODS

Facies analysis relied on the sedimentological characterization of 24 sediment cores and stratigraphic interpretation of 38 piezocone penetration tests along two transects in the Argenta–Longastrino area (Fig. 1A). In order to enhance stratigraphic interpretation, a coring survey was carried out between May and October 2018, and four continuous cores (B1 to B4 in Figs 1A and 2), 17 to 40 m long, were investigated in detail. Cores B1 to B4 were recovered through a continuous perforating system that guaranteed an undisturbed stratigraphy and high recovery percentages (>90%). Cores were split lengthwise and described for grain size, colour, organic-matter content, style of stratigraphic contact (transitional, sharp and erosional), accessory materials

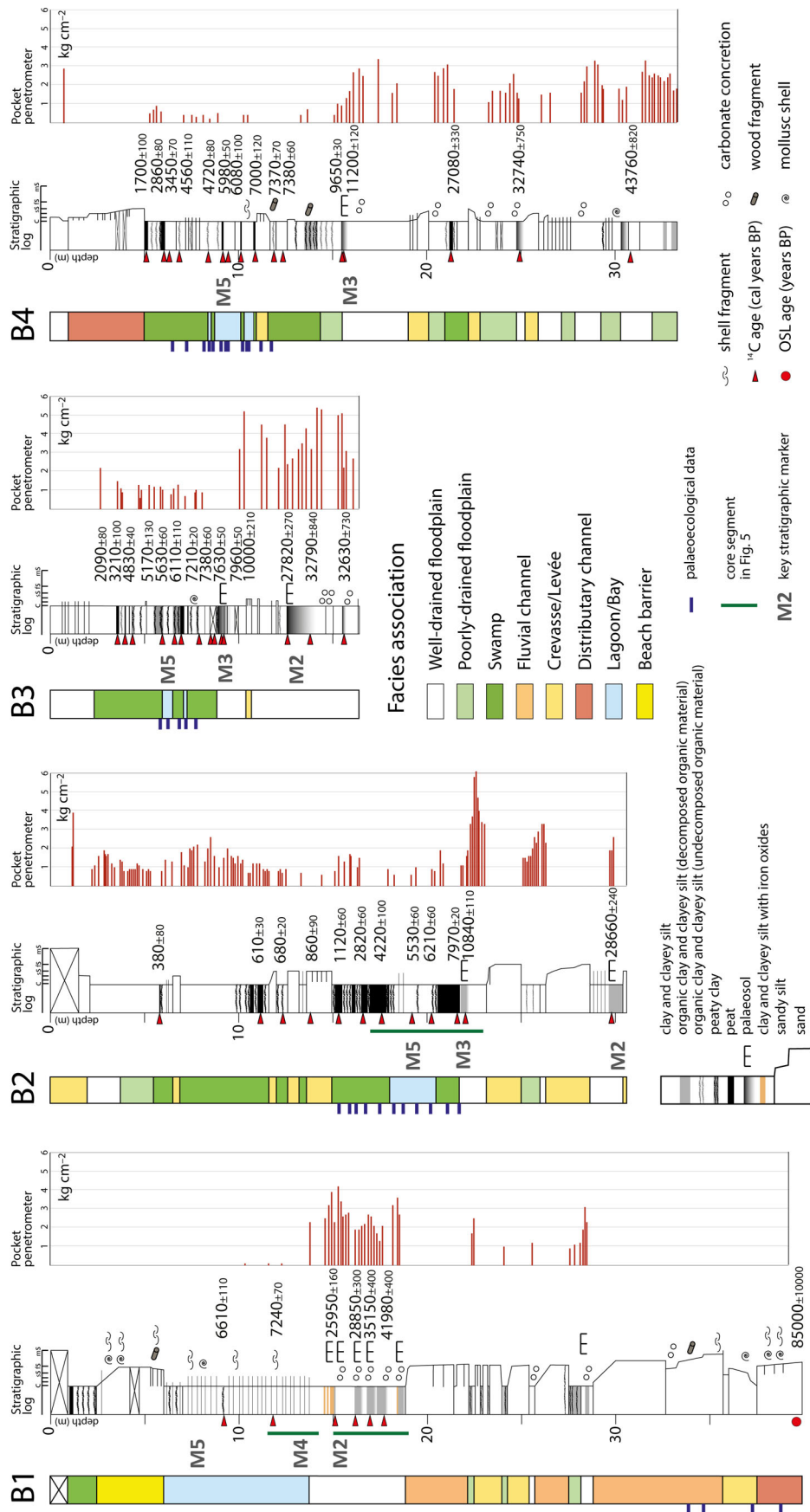


Fig. 2. Detailed stratigraphy and facies interpretation of cores B1 to B4 (see Fig. 1 for location). Stratigraphic markers of Figs 4 and 5 are indicated.

(vegetation remains, woods, roots, bioturbation, Fe-Mn oxides, carbonate nodules and pedogenic features), and faunal content. Pocket penetration measurements, a quick and inexpensive tool that may enhance stratigraphic interpretation of fine-grained Quaternary deposits (Amorosi *et al.*, 2015), supplied additional information about geotechnical characteristics of the study units. Because of the generally poor preservation of sedimentary structures, cores were subdivided into facies associations, rather than sedimentary facies.

Microfossil associations provide excellent palaeoenvironmental information for core analysis, far greater than can be obtained from traditional sedimentological investigations, especially in mud-prone sedimentary successions. In this study, palaeontological data, mainly based on foraminifera and ostracoda, highlighted subtle changes in depth, salinity, degree of confinement, oxygen and food availability in the depositional environment (e.g. Debenay *et al.*, 2000; Murray, 2006; Barbieri & Vaiani, 2018; Barbieri *et al.*, 2019). Comparison with spatial distribution patterns of the modern meiofauna helped to define the boundaries of lithologically homogeneous facies assemblages and was useful to constrain and correlate sediment packages on a basin scale (Campo *et al.*, 2017; Amorosi *et al.*, 2020). Thirty-three samples were analyzed for characterization of facies associations in cores B1 to B4 (Fig. 2). In addition, 89 samples were collected from Holocene (41 samples) and Last Interglacial (48 samples) coastal and paralic deposits of cores 204-S3 and 222-S2. These new data were integrated by a review of published palaeontological analyses from cores 204-S5, 204-S17, 205-S1, 205-S2, 205-S4, 205-S10 and 222-S2 (Amorosi *et al.*, 2003, 2004, 2005; Geological Map of Italy Sheet 222 'Lugo').

Stratigraphic correlation relied upon a total of 102 radiocarbon dates (Table S1). The ^{14}C database includes a set of 39 published dates (Preti, 1999; Amorosi *et al.*, 2003, 2005, 2017a, 2020; Bruno *et al.*, 2019; Geological Map of Italy Sheets 204 'Portomaggiore' and 222 'Lugo') and 63 unpublished radiocarbon dates. Radiocarbon dating on 49 samples from cores B1 to B4 (Fig. 2) was performed at KIGAM laboratory (Daejeon City, Republic of Korea) on wood, plant fragments, peat and shells (Table S1). The calibration of conventional radiocarbon ages was based on the IntCal13 dataset (Reimer *et al.*, 2013) using OxCal 4.3. (Bronk Ramsey, 2009). Before AMS counting, organic samples (for example, wood) were pre-

treated with the acid-alkali-acid method in order to remove CaCO_3 and humic-acids contamination. Shell samples were subjected to HCl etches to eliminate secondary carbonate component. Soil and peat samples were treated with 0.5 M NaOH at 80°C for 2 h to extract humic acid without extraction of the humin fraction. Humic acids were then collected by adding concentrated hydrochloric acid to the solution.

Beyond the limits of radiocarbon dating, age determinations included one sample dated by optically stimulated luminescence (OSL), along with two published electron spin resonance (ESR) dates (samples K-4383 and K-4385 in Ferranti *et al.*, 2006) coupled with a long-cored pollen profile (core 222-S2 in Geological Map of Italy Sheet 222 – 'Lugo'). Optically-stimulated luminescence (OSL) dating from bottom core B1 was carried out at the Luminescence Dating Laboratory of the University of Oxford, UK. The sample destined for OSL dating was recovered during drilling operations with an Oesterberg cell. A 60 cm core segment was removed and the exposed top and bottom parts were then sealed with paraffin. Subsequently, the paraffin caps were removed in a dark room and the upper and lowermost 5 cm of the sample were discarded. The innermost part of the core segment was stored in lightproof containers. Measurements were performed on small quartz multigrain aliquots ($n = 30$) with standard automated luminescence readers made by Risø and Freiberg Instruments (Risø Kagaku Corporation, Tokyo, Japan; Freiberg Instruments GmbH, Freiberg, Germany) using a double SAR post-IR blue or post-IR Green OSL measurement protocol. Dose rate calculations are based on Aitken (1985) and are derived from the concentrations of radioactive elements (potassium, rubidium, thorium and uranium) within the sediment sample (s). These were derived from elemental analysis by ICP-MS/AES using a fusion sample preparation technique. The final OSL age estimate includes an additional 4% systematic error to account for uncertainties in source calibration and measurement reproducibility. Dose rate calculations were obtained using dose rate conversion factors of Guerin *et al.* (2011) and calculated using the DRAC software (v1.02) developed by Durcan *et al.* (2015). The contribution of cosmic radiation to the total dose rate was calculated as a function of latitude, altitude, burial depth and an average over-burden density of 1.9 g cm^{-3} based on data by Prescott & Hutton (1994).

Location, data of the event, and magnitude of historical earthquakes (Fig. 1A and Table S2)

are from the Parametric Catalogue of Italian Earthquakes 2015 (CPTI15 in Rovida *et al.*, 2019). This catalogue, produced by *Istituto Nazionale di Geofisica e Vulcanologia* (INGV), is available via its open-access website (https://emidius.mi.ingv.it/CPTI15-DBMI15/index_en.htm). The CPTI15 includes homogeneous macroseismic and instrumental data and parameters for Italian earthquakes with maximum intensity ≥ 5.0 or magnitude ≥ 4.0 in the period 1000 to 2014 AD. Additional instrumental data were taken from ISIDe (ISIDe Working Group INGV, 2015). The focal mechanisms of instrumental events associated with the Ferrara arc are reported by Martelli *et al.* (2017).

FACIES ASSOCIATIONS

Eight major facies associations were recognized from core deposits of the Po Plain (Fig. 3). They represent alluvial to paralic and nearshore

depositional environments. Characterization of lithofacies assemblages relied upon combined sedimentological and palaeoecological core analysis. For offshore/prodelta deposits, which were not encountered in the newly drilled sediment cores B1 to B4, sedimentological description and interpretation are based on literature data (Amorosi *et al.*, 2017a, 2019; Bruno *et al.*, 2017b). Facies associations are described from proximal to distal locations.

Fluvial-channel facies association

Description

This facies association consists of moderately sorted, medium to coarse sand bodies (Fig. 3A), with erosional base, characteristic fining-upward (FU) trend and generally sharp top. Vertically amalgamated, multi-storey bodies with faint traces of unidirectional, high-angle cross-stratification are up to 10 m thick (Fig. 2). Near the base of sets, the sand is coarser and may contain

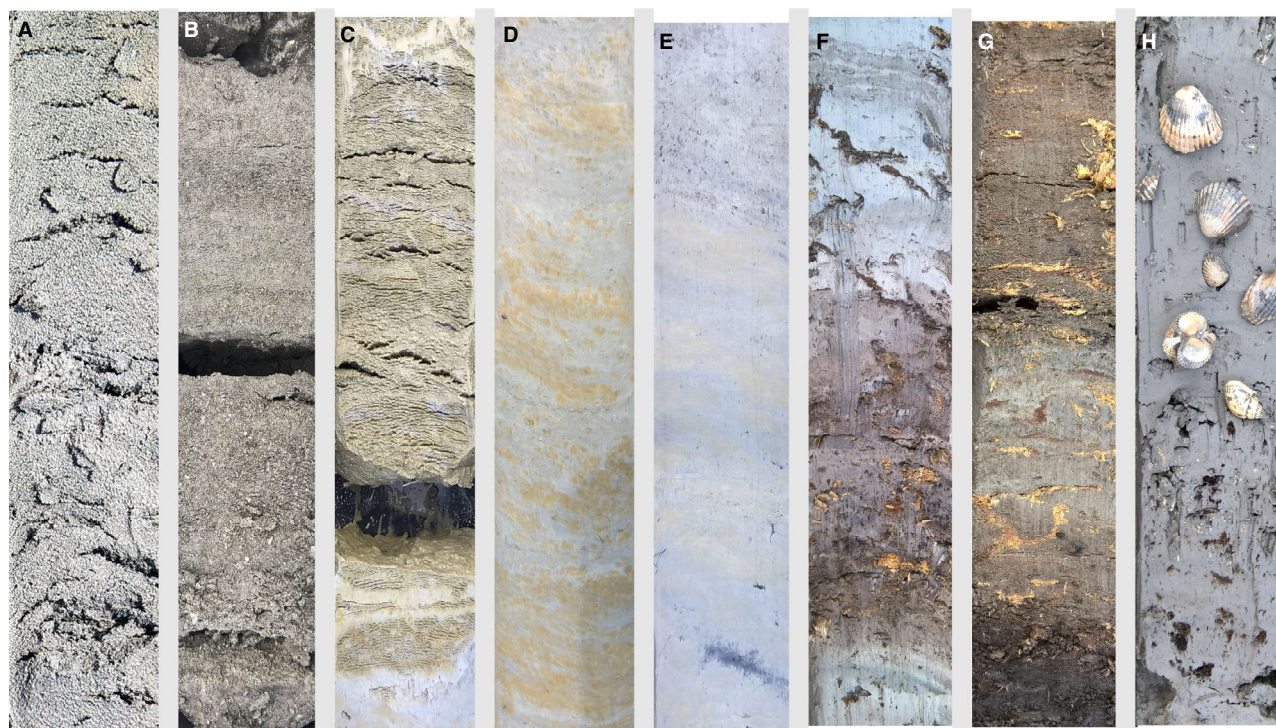


Fig. 3. Representative core photographs of major facies associations in the study area. (A) Fluvial-channel, coarse-grained sand (core B1, 29.0 to 29.4 m depth). (B) Distributary-channel medium to fine sand, with fining-upward trend and shell fragments (core B1, 38.6 to 39.0 m depth). (C) Crevasse silty-sand layer (core B2, 6.5 to 7.0 m depth) onto floodplain deposits. (D) Varicoloured, well-drained floodplain silt and clay (core B1, 14.4 to 14.9 m depth). (E) Poorly-drained floodplain silt and clay with organic matter (core B2, 7.2 to 7.7 m depth). (F) Organic-rich, swamp clay (core B2, 10.3 to 10.8 m depth). (G) Swamp peat (core B2, 17.3 to 17.8 m depth). (H) Lagoonal clay (facies 2) with abundant *Cerastoderma glaucum* shells (core B2, 19.2 to 19.7 m depth). Core width in the photographs is 10 cm. For core locations, see Fig. 1A.

abundant granules. Finer-grained (silt and clay) deposits are highly subordinate and thin mud interbeds locally separate individual sand units. Wood fragments are locally dispersed. The meiofauna includes rare fragments of freshwater ostracods. Individual FU sequences commonly show upward transition to organic-rich layers (Fig. 2).

Interpretation

Given the general poor recovery of loose sand in cores and the inherent difficulty of preserving sedimentary structures, interpretation of this facies association is based on the distinctive combination of lithology, style of stratigraphic contacts, body fossils and accessory components. The erosional lower boundary of this facies association, combined with its thickness, FU trend and rare presence of freshwater fossils, are all characteristic features of fluvial-channel deposits. Thicker, composite channel bodies, resulting from the amalgamation of individual sand bodies are interpreted to be part of laterally extensive fluvial channel-belts (Amorosi *et al.*, 2017b). The upward transition to organic-matter rich deposits indicates abandonment of river channels, probably occurring in response to avulsion events.

Distributary-channel facies association

Description

This facies association shares some common characteristics with the fluvial-channel facies association, such as lithology (sand is dominant), erosional lower boundaries and FU grain-size trends (core B1 in Fig. 2). This unit is distinct, however, from the fluvial-channel facies association by its generally finer grain size (Fig. 3B) and thickness (invariably <5 m), concurrent with a higher abundance of thin mud intercalations and drapes, and the common presence of wood fragments. A diagnostic feature of this facies association is the local abundance of marine shell fragments (Fig. 3B). This unit is commonly associated with, or intercalated between, organic-rich layers and peats (Fig. 4).

Interpretation

Based on grain size and on the abundance of shell fragments, this facies association is interpreted to represent a high-energy deposit in a comparatively more distal environment than a fluvial channel, locally subject to a marine influence, such as a distributary channel. This interpretation, which is corroborated by recent

mapping of Holocene distributary-channel systems in the area (Bruno *et al.*, 2019), is also in good agreement with the abundance of wood within bar deposits. The relatively lower thickness of this facies association, in contrast to the fluvial-channel counterpart, suggests a lack of multi-storied architecture, which is typical of coastal and delta plains.

Crevasse/levée facies association

Description

This facies association, 0.5 to 3.5 m thick (Fig. 2), is invariably associated with alluvial deposits and consists largely of medium to fine varicoloured sands and silts, alternating in various proportions. A common lithofacies consists of very fine to medium-grained sand layers, a few decimetres thick, that form thin sand bodies, generally less than 1 m thick, that overlie thick silt and clay units. Sand bodies may display either a fining-upward trend, with a sharp base and gradational top (Fig. 3C), or a coarsening-upward trend, with gradational lower boundary and sharp top. This facies association can exhibit the rhythmical alternation of centimetre-thick layers of very fine sand, silt and clayey silt, with abundant plant debris and the presence of rootlets. Sand layers, in this case, invariably display sharp lower boundaries.

Interpretation

Interpretation of this facies association relies mostly upon the vertical stratigraphic relation with alluvial deposits, combined with the common occurrence of indicators of subaerial exposure (rootlets and plant debris) and a lack of fossils. Sand bodies with a sharp base and internal FU trends are interpreted to reflect crevasse-channel deposits, whereas CU trends and gradational lower boundaries are diagnostic of distal crevasse splays. Thinly interbedded lithologies (sand–mud couplets) recording centimetre-scale units are considered, instead, levée deposits (Hobday, 1978).

Well-drained floodplain facies association

Description

This facies association, >6 m thick (Fig. 2), is a monotonous succession of rooted, bioturbated, and locally hardened silt and clay with highly subordinate (<10%) sand intercalations. Plant debris and decomposed organic matter are common accessory constituents. Yellow, brownish and

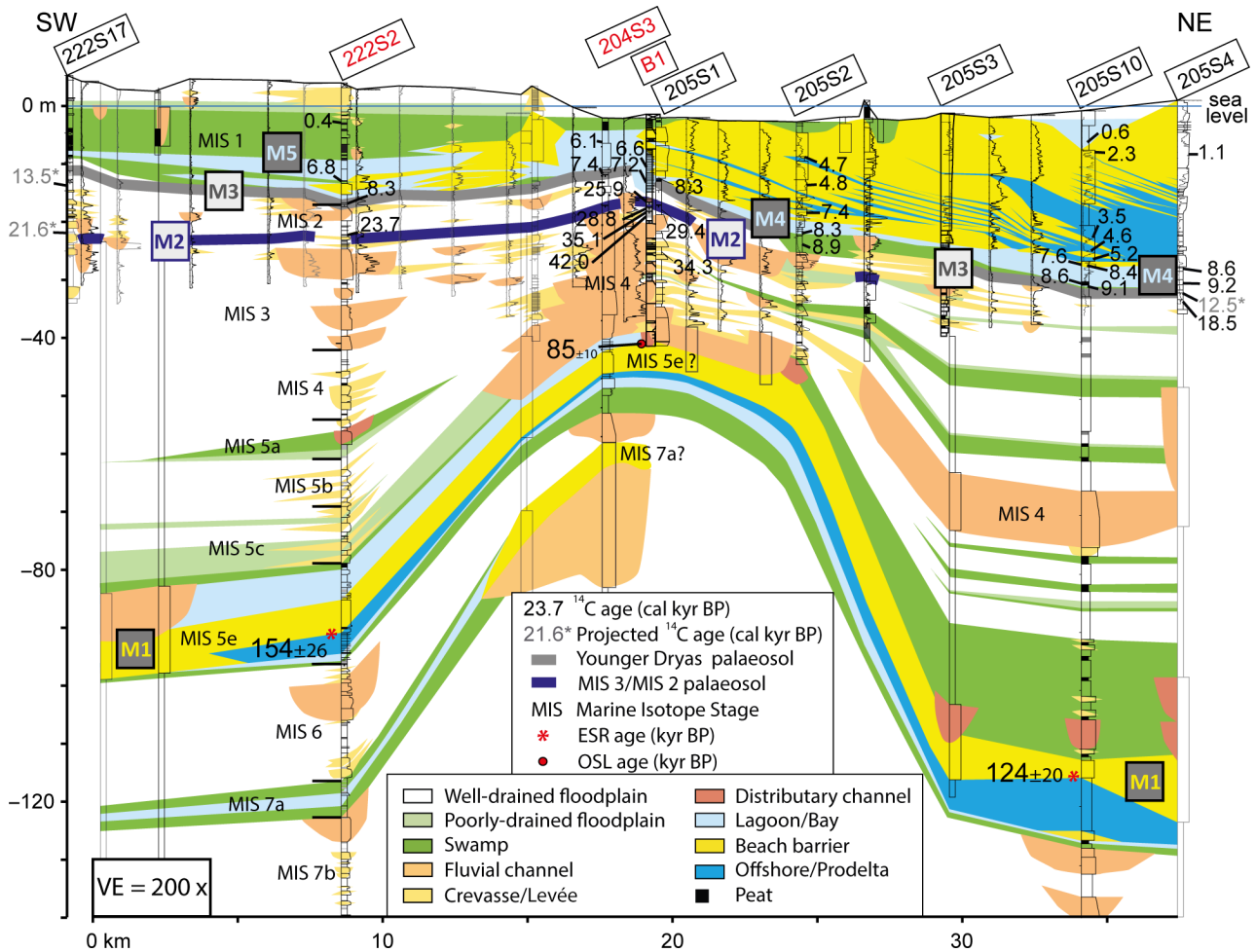


Fig. 4. Stratigraphic correlation panel showing deformation of marker horizons M1 to M4 in the Longastrino area (for location of cores – boxed – and CPTU tests, see Fig. 1). New cores analysed for palaeontology are marked in red. ESR absolute ages in cores 222-S2 and 205-S10 are from Ferranti *et al.* (2006). For detailed stratigraphy of core B1, see Fig. 2. VE, vertical exaggeration.

black mottles due to Fe and Mn oxides make this mud typically varicoloured (Fig. 3D). Horizons with dark grey, organic-rich clay and silt layers overlying light grey horizons with calcite nodules and slickensides, are commonly observed. This facies association is generally barren or may contain at most a few opercula of freshwater gastropods. Pocket penetration values range between 1.5 kg cm^{-2} and 6.0 kg cm^{-2} (Fig. 2).

Interpretation

This facies association is inferred to reflect a low-energy, continental depositional environment dominated by suspension fall-out, with highly subordinate traction processes. Segregation of iron and manganese oxides as mottles or concretions indicates alternating reducing and oxidizing

conditions during episodic or seasonal water saturation in a vadose zone (Kraus & Aslan, 1993). Abundant root fragments, preserved undifferentiated organic matter and carbonate concretions represent common pedogenic features, typical of weakly developed palaeosols, such as Inceptisols (Soil Survey Staff, 1999) and as a whole are evidence of subaerial exposure (see next section). Overconsolidated silt and clay layers, exhibiting compression values $>3.5 \text{ kg cm}^{-2}$, higher than typically unconsolidated Quaternary deposits, are likely to reflect secondary consolidation due to ageing and desiccation and are interpreted as palaeosols (Amorosi *et al.*, 2015). This facies association, in general, is inferred to reflect over-bank fines deposition in a flood basin with a relatively low groundwater table.

Poorly-drained floodplain facies association

Description

This facies association, generally less than 2 m thick (Fig. 2), consists of soft silt and subordinate clay, with a uniform grey colour (Fig. 3E). Compared to its well-drained counterpart, this lithofacies assemblage has rare carbonate concretions and lacks pedogenic features. Concentration of organic matter is locally observed (Fig. 3E). Shell fragments of freshwater–oligohaline molluscs, including *Hydrobia* and *Planorbis*, and freshwater ostracods, such as *Candona* and *Ilyocypris*, can be abundant. Pocket penetration tests generally record poor consolidation, with values in the range of 0.9 to 2.3 kg cm⁻² (Fig. 2). This facies association is vertically associated with organic-rich layers and swamp peats (Fig. 2).

Interpretation

The homogeneous grey colour, a lack of brownish and yellowish alteration colours and local association with organic-rich layers suggest that deposition of this facies association took place in a poorly-drained flood basin with lack of oxidation and with a high groundwater table. Useful keys for discrimination of this facies association are the lack of palaeosols and the low compression values: both features, along with the occurrence of freshwater fossils, suggest sedimentation in topographically low, frequently submerged depositional environments with only very short phases of subaerial exposure, such as ephemeral ponds and swamps (Guccione *et al.*, 2009). Poorly drained conditions and waterlogging likely prevented the formation of soils and indurated layers.

Swamp facies association

Description

This facies association, up to 10 m thick (Fig. 2), is composed of very soft, grey to dark grey clay, with an abundance of wood and plant debris that can be scattered or concentrated in discrete horizons (Fig. 3F). Dark brown peat-rich intervals, with subordinate clay material, are commonly observed (Fig. 3G). Freshwater ostracods, including *Candona* and *Pseudocandona*, and subordinate *Ilyocypris* typify this facies association. Pocket penetration values are generally low and range between 0.2 kg cm⁻² and 1.5 kg cm⁻² (Fig. 2).

Interpretation

This facies association records deposition of fine-grained sediment and organic matter in a

stagnant, freshwater environment that received abundant organic detritus. Black to dark grey colours owe their origin and distinctiveness to finely disseminated organic matter, and possibly iron sulphide, darkness being a function of high amounts of organic carbon. The fossil content suggests that this lithofacies assemblage formed in semi-permanently flooded wetlands (Salel *et al.*, 2016; Campo *et al.*, 2017), as part of inner estuarine or upper delta plain environments (Amorosi *et al.*, 2017a; Bruno *et al.*, 2019).

Lagoon/bay facies association

Description

This facies association is up to 6 m thick (Fig. 2) and typically associated with swamp deposits. It consists of thoroughly bioturbated, highly fossiliferous grey silty clay and clay, with rare vegetal remains, and it lacks oxides and carbonate concretions. Mollusc shells are mostly represented by *Cerastoderma glaucum* (Fig. 3H), but *Abra segmentum*, *Loripes orbiculatus* and *Ecrobia ventrosa* are commonly encountered (Scarponi *et al.*, 2017). Based on combined lithological and palaeoecological attributes, three sedimentary facies were distinguished. Facies 1 is a homogeneous grey clay with abundant organic debris and wood fragments, dominated by the benthic foraminifera *Trochammina inflata*. Facies 2 is a highly fossiliferous, homogeneous grey clay (Fig. 3H), with scattered wood fragments and an abundance of the ostracod *Cypri-deis torosa* and benthic foraminifera *Ammonia tepida*, *Ammonia parkinsoniana* and *Haynesina germanica*. Facies 3 includes thinly bedded (<3 cm), sharp-based alternations of normal graded fine sand and clay, with abundant mollusc fragments concentrated at the base of individual sand layers. The meiofauna exhibits a high species diversity, with the dominance of *Ammonia tepida* and *Ammonia parkinsoniana* and the occurrence of poorly preserved, lagoon to shallow-marine foraminifera (for example, *Aubignyna perlucida*, *Porosononion granosum*, *Miliolinella* spp. and *Quinqueloculina seminula*). Pocket penetration tests yielded values in the range of 0.2 to 1.0 kg cm⁻² (Fig. 2).

Interpretation

In the Po River system, freshwater/hypohaline deposits transform seaward to a wide range of facies typical of brackish environments behind a barrier complex, as part of an outer, wave-dominated estuary or a lower delta plain (Amorosi

et al., 2017a, 2020; Bruno *et al.*, 2017b). The fossil content of this facies association clearly indicates a depositional environment fed by mixed marine and fluvial water sources in a microtidal regime (Scarponi *et al.*, 2013). Based on the diagnostic meiofauna, facies 1 is believed to reflect an inner lagoon sub-environment (Debenay & Guillou, 2002). The brackish oligotypic fauna of facies 2, able to tolerate frequent changes in salinity, is a reliable indicator of a permanently submerged, semi-enclosed brackish-water basin subject to salinity variations, such as a central lagoon sub-environment (Barbieri & Vaiani, 2018). Relatively open, brackish to marine conditions are recorded by the heterolithic facies 3 (Debenay *et al.*, 2000). Sand–mud alternations with a transported shallow-marine meiofauna are interpreted to reflect the distal fringe of a flood-tidal delta or a washover fan.

Beach-barrier facies association

Description

This facies association is poorly represented in cores B1 to B4 (Fig. 2). It consists of well-sorted, fine to coarse sand and is typified by a highly diversified marine fossil assemblage, with an abundance of fragmented marine mollusc shells (mostly *Donax* and *Lentidium mediterraneum*). Foraminifera and ostracoda are generally abraded and grain-size sorted: they consist predominantly of *Ammonia beccarii*, *Elphidium* spp. and *Pontocythere turbida*. Sedimentary structures are poorly preserved. Mud layers are extremely rare.

Interpretation

The characteristic sandy deposit (i.e. lack of mud) and the variety and abundance of mollusc shells associated with a typically shallow-marine microfauna, all point to a high-energy, coastal palaeoenvironment, such as a beach barrier. The mixture of nearshore species and the common occurrence in the meiofauna of poorly-preserved and size-selected specimens suggests hydraulic sorting by waves and longshore currents. Poor preservation of sedimentary structures precludes a clear differentiation between distinct sedimentary facies. However, finer-grained sand with fewer (and smaller) body fossils is interpreted to represent lower shoreface deposits, whereas medium-coarse sand with an abundance of shells is considered to be upper shoreface or foreshore deposits. Oligotypic assemblages of *Lentidium mediterraneum*

indicate river-influenced (mouth bar) settings (Scarponi *et al.*, 2017).

Offshore/Prodelta facies association

This facies association, which is not represented in cores B1 to B4, has been widely described from other cores in the area (Amorosi *et al.*, 2019). It consists of interlayered, millimetre to centimetre-thick grey silt to clay couplets, with highly subordinate, sharp-based sand layers (sand proportion is <2%). In facies 1, muds are moderately to heavily bioturbated and have a mottled texture. Primary sedimentary structures, such as small wave ripples, are locally preserved. The foraminiferal assemblage exhibits high species diversity, with variable amounts of *A. parkinsoniana*, *A. tepida*, *Aubignyna perlucida*, *Criboelphidium* spp., *Elphidium* spp., *Textularia* spp. and a variety of miliolids, accompanied by subordinate hyaline epiphytic taxa. The ostracod fauna includes large amounts of *Semicytherura* spp. and *Loxococoncha* gr. *rhomboidea*, along with *Cytheridea neapolitana*, and *Pontocythere turbida*. In facies 2, muds are finely laminated, with low bioturbation levels and commonly abundant plant and other organic matter. Occasional thin-bedded intercalations of very fine to fine sand, with sharp base and FU trend, are observed. The meiofauna is dominated by opportunistic foraminifer and ostracod species, such as *A. parkinsoniana*, *A. tepida*, *A. perlucida*, *N. turgida*, *P. granosum*, *Palmococoncha turbida* and *Leptocythere ramosa*.

Interpretation

Clay-sized material, paucity of sand and an abundance of marine fossils clearly reflect sedimentation in a low-energy, shallow-marine environment, below fair-weather wave base. In facies 1, high bioturbation levels indicate intense biogenic activity under conditions of low sedimentation rates. An offshore environment is suggested by highly diversified assemblages and by the common occurrence of open-marine taxa (i.e. *Textularia* spp. and *Cytheridea neapolitana*) that indicate the deepest water depths in the study area (Rossi & Vaiani, 2008; Rossi, 2009; Dasgupta *et al.*, 2020). The local abundance of *A. tepida* and *A. perlucida* provides evidence for a temporary increase in fluvial influence (Jorissen, 1988; Goineau *et al.*, 2011). In facies 2, low bioturbation levels and a meiofauna able to tolerate stressed marine conditions, including

high nutrient flux and turbidity (Jorissen *et al.*, 2018; Barbieri *et al.*, 2019), suggest sedimentation in a prodelta environment, in front of a river mouth. Local abundance of *Nonionella turrida* documents ample food availability and oxygen deficiency at the sea bottom (e.g. Van der Zwaan & Jorissen, 1991), which are indicative of a distal prodelta or a mud belt setting. Abundant plant material suggests derivation from land (e.g. Bohacs *et al.*, 2014), whereas thin sand–silt couplets with a sharp base and FU trend are interpreted to reflect river-generated hyperpycnal flows (Bhattacharya & MacEachern, 2009; Schieber, 2016).

KEY STRATIGRAPHIC MARKERS

High-resolution stratigraphic data for the study area are presented on two cross-sections (Figs 4 and 5), where stratigraphic logs and piezocone

penetration tests have average spacing of *ca* 1000 m. To identify diagnostic marker horizons in the study succession and track them in the subsurface, sediment core stratigraphy was evaluated according to eight criteria: sedimentary characteristics; palaeontological content; age; geotechnical properties; stacking patterns of facies; lateral facies variations; stratigraphic position relative to other marker beds; and sequence-stratigraphic significance (Amorosi *et al.*, 2017a). Stratigraphically distinct key horizons of regional significance were found at five correlatable levels (M1 to M5 in Figs 2, 4 and 5). Three of these (M1, M4 and M5) formed in a low-gradient coastal environment and thus represent almost flat surfaces at the time of deposition. Precise chronological constraints to markers M2 to M5 derive from a total of 102 radiocarbon dates (Table S1).

Although individual key beds can be clearly identified on a regional scale, they are not

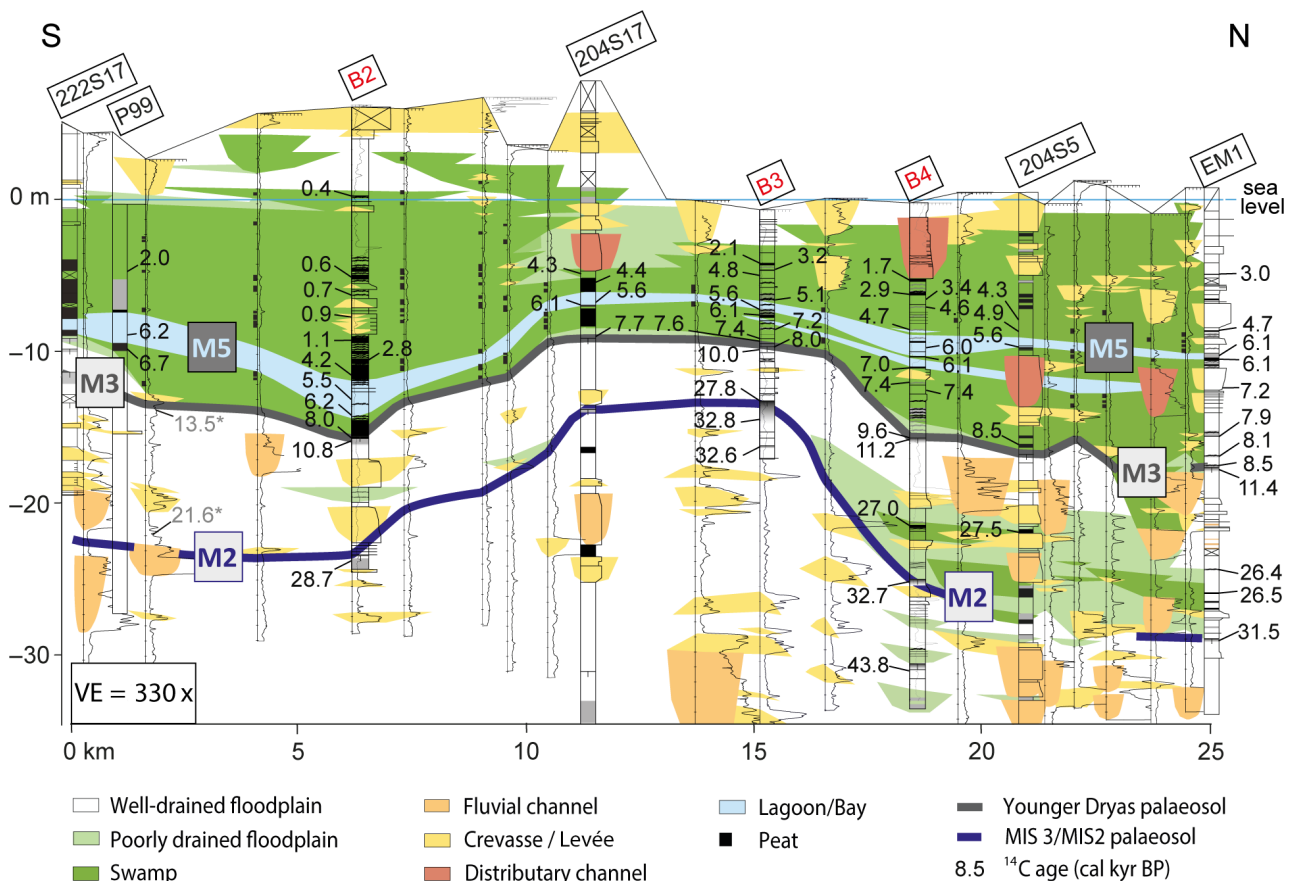


Fig. 5. Stratigraphic correlation panel showing deformation of marker horizons M2, M3 and M5 in the Argenta area (for location of cores – boxed – and CPTU tests, see Fig. 1). New cores analysed for palaeontology are marked in red. For detailed stratigraphy of cores B2, B3 and B4, see Fig. 2. VE, vertical exaggeration.

ubiquitous and were not observed in all cores. For example, lagoonal horizons may grade locally into swamp or beach-barrier facies associations. On the other hand, weakly developed palaeosols formed onto silty and clayey (flood-plain) substrates, whereas they were not observed onto coeval sandy crevasse and levée deposits.

For simplicity, stratigraphic markers will be subsequently denoted in chronological order.

Marker M1: Last Interglacial (MIS 5e) beach deposits

Last Interglacial (MIS 5e) beach-barrier deposits (marker M1) form a fossiliferous sand body of regional significance, 10 to 15 m thick, that extends continuously in south–north direction, parallel to the shoreline, and about 40 to 50 km along dip (Amorosi *et al.*, 2004; Campo *et al.*, 2020b). This wedge-shaped sediment body formed in just a few thousand years in response to coastal progradation, when global mean sea-level reached a peak of 5 to 9 m above present-day sea level, during the MIS 5e highstand (O'Leary *et al.*, 2013).

The MIS 5e coastal wedge can be easily identified in core data, because it is a shell-rich sand body (Fig. 6A) sandwiched between non-marine deposits (Campo *et al.*, 2020b). Although this sand body accumulated in a variety of coastal sub-environments that may span several metres in depth along the coast profile, marked differences in depth make it an excellent stratigraphic marker at the basin scale (Fig. 4). Chronological constraints to MIS 5e arise primarily from the following features:

1 Detailed pollen profiles from core 222-S2 (Geological Map of Italy – Sheet 222 'Lugo') and other pollen spectra from the same area (Amorosi *et al.*, 2004) provide a clear MIS 5e age attribution to Marker M1 (Fig. 4). The base of MIS 5e deposits, in particular, is marked by a major peak in pollen concentration, associated with an abrupt upward increase in mixed deciduous broad-leaved vegetation, dominated by *Quercus*, and a concomitant decrease in *Pinus* and shrubby–herbaceous communities (Amorosi *et al.*, 2004). A similar signal has been reported from several European pollen series (Helmens, 2014).

2 Two ESR absolute ages obtained from marine mollusc shells of cores 222-S2 and 205-S10

(Ferranti *et al.*, 2006 – Fig. 4) agree with an MIS 5e age assignment.

3 Marker M1 is the first marine deposit encountered below the Holocene succession: its stratigraphic position thus is consistent with an age attribution to the Last Interglacial.

4 Vertical patterns and the spatial distribution of depositional systems above Marker M1 invariably denote the presence of a thick alluvial succession with no intervening brackish or marine deposits, which is in good agreement with sedimentation during a prolonged phase of generalized sea-level drop (MIS 4–2 interval).

In the rapidly subsiding Po Basin, the top of marker M1 commonly occurs at depths of 90 to 110 m (Fig. 4). In sharp contrast, Pleistocene sands containing a marine microfauna were identified in this study from the Longastrino area, at depths of just 40 m (cores 204-S3 and 205-S1 in Fig. 4). In core B1, an OSL date from a distributary-channel deposit just above the marine sands yielded an age of 85 ± 10 kyr BP (Fig. 4), consistent with an MIS 5a to MIS 5c age attribution. It is remarkable that MIS 5a to 5c deposits in core 222-S2 are considerably deeper than coeval units in core B1 (Fig. 4).

Given that the MIS 5e nearshore sand body provides a reasonably accurate assessment of palaeo-sea-level position with an uncertainty <8 m (Ferranti *et al.*, 2006), the Longastrino ridge between cores 204S3 and 205S1 accommodates 40 to 60 m of vertical separation from anticline to syncline positions (Fig. 4).

Markers M2 and M3: Upper Pleistocene palaeosols (29 to 24 cal kyr BP and 13 to 11 cal kyr BP)

Two pedogenically modified horizons of Late Pleistocene age (M2 and M3 in Figs 4 and 5) represent key stratigraphic markers across the upper Quaternary succession of the Po Plain, because of their basin-wide occurrence and very high correlation potential (Morelli *et al.*, 2017; Amorosi *et al.*, 2017b). These weakly developed palaeosols, which are part of the well-drained floodplain facies association, exhibit distinctive A-Bk, A-Bw or A-Bk-Bw profiles (Inceptisols) that make them easily recognizable in cores within the thick non-marine Upper Pleistocene succession (Fig. 6B and C). Soil profiles are typified by: (i) topmost dark grey/black ('A') horizons, with no reaction to hydrochloric acid, that reflect accumulation of organic matter and

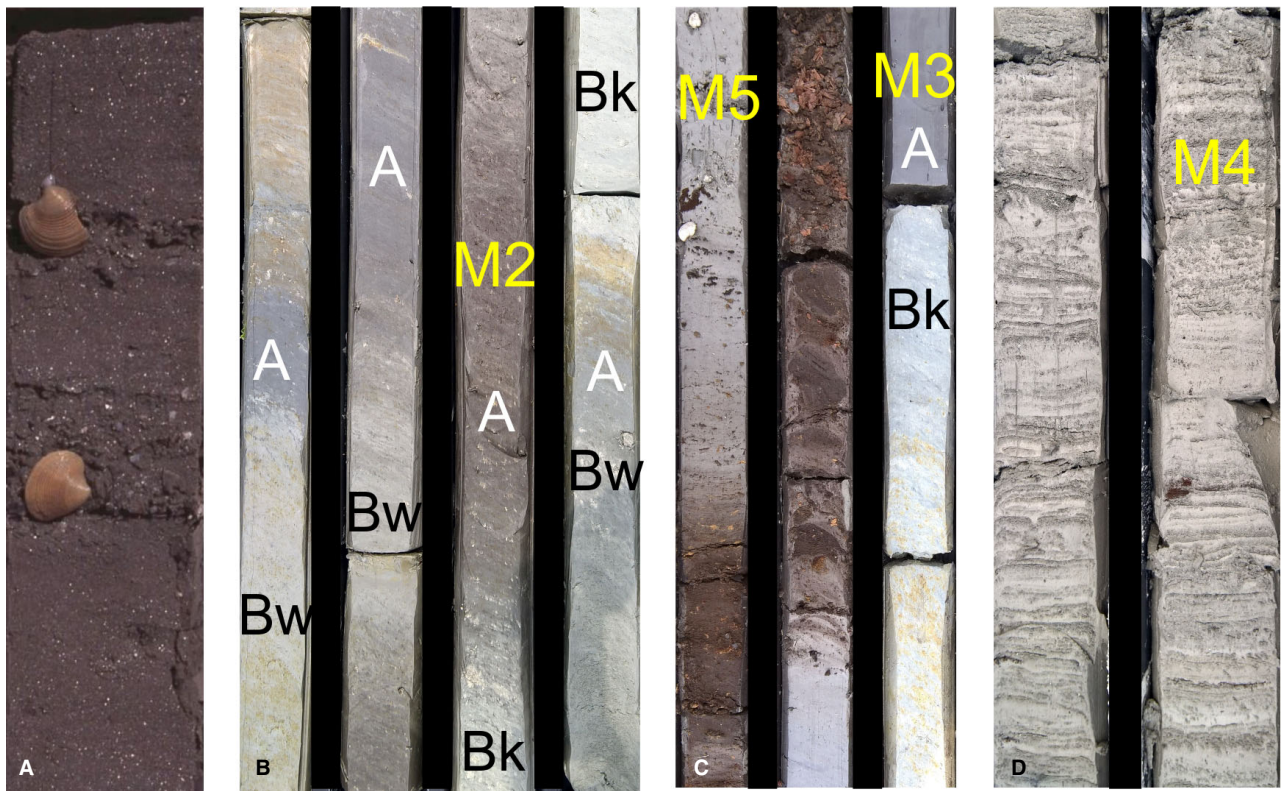


Fig. 6. Representative core photographs of key stratigraphic horizons M1 to M5: (A) Last Interglacial (MIS 5e) lower shoreface (beach-barrier) fine sands, with abundant mollusc shells (marker M1: core 223-S12, 117 to 118 m depth – from Amorosi *et al.*, 2004); (B) vertically stacked, multiple Upper Pleistocene Inceptisols (marker M2: core B1, 15 to 19 m depth) and their related soil horizons ‘A’, ‘Bw’ and ‘Bk’; (C) Inceptisol marking the Pleistocene–Holocene boundary (marker M3, and related soil horizons ‘A’ and ‘Bk’), overlain by a thick swamp peat interval and *Cerastoderma glaucum*-rich lagoon grey clay (marker M5) (core B2, 20 to 23 core depth); (D) bioturbated, lagoonal (facies 3) clay-sand alternations (marker M4: core B1, 12 to 14 m depth). Core bottom is lower right corner. Core width in the photographs is 10 cm. For core locations, see Fig. 1A.

leaching of CaCO_3 ; (ii) lower, light grey, Ca-enriched (‘Bk’) horizons, with yellow-brownish mottles due to Fe and Mn oxides, that indicate fluctuating redox conditions with iron dissolution and redeposition (Fig. 6B and C). Soil layers with subtle evidence of weathering (for example, oxidation, root traces and reaction to HCl) were interpreted as ‘Bw’ horizons.

Markers M2 and M3 have clear sequence-stratigraphic significance: marker M2 represents the sequence boundary of the Last Glacial Maximum depositional sequence (Amorosi *et al.*, 2017b), whereas top marker M3 is the transgressive surface (Amorosi *et al.*, 2017a). These two palaeosols are also clearly identified by their geotechnical properties, as they both represent well-indurated horizons with high compression values, between 3.5 kg cm^{-2} and 6.0 kg cm^{-2}

(Fig. 2). The diagnostic geotechnical signature of these stiff layers was also recognized through the analysis of piezocone penetration tests (Amorosi & Marchi, 1999).

Palaeosols M2 and M3 have been chronologically anchored to temporally discrete palaeoclimatic events that coincide with rapid shifts from relatively warm to colder phases (Bruno *et al.*, 2020). In particular, M2 caps a set of closely-spaced, weakly developed palaeosols (Fig. 6B) and spans approximately 29 to 24 kyr BP. It is interpreted to reflect a phase of stepped channel entrenchment that took place across the MIS 3/2 transition, culminating at the onset of the Last Glacial Maximum (Amorosi *et al.*, 2017b). Palaeosol M3 was formed, instead, around the Pleistocene–Holocene boundary (13 to 11 cal kyr BP) and correlates, in particular, to

the short-lived Younger Dryas cold event. Correlation of markers M2 and M3 relies on radiocarbon-dated bulk-sediment samples from palaeosols and on wood and peat from the overlying and underlying overbank facies.

Palaeosols M2 and M3 exhibit large differences in depth across the study area, in the range of 10 m (M3) to 15 m (M2) (Figs 4 and 5). In the Longastrino area, close to core B1 (Fig. 5), the folding of M2 and M3 coincides with the underlying deformation of the coastal marker M1 (Fig. 4). The relatively short-lived exposure age of palaeosols M2 and M3 resulting from ^{14}C ages (<5000 years – Figs 4 and 5) allows their approximation to isochronous surfaces and their use as powerful (quasi-synchronous) chronostratigraphic indicators. However, palaeosols M2 and M3 may reflect irregular palaeo-reliefs, which represents a main limitation on their use to quantify strata deformation.

Markers M4 and M5: Holocene lagoon deposits (8.6 to 8.3 cal kyr BP and 6.2 to 5.6 cal kyr BP)

Transgressive deposits of Early–Middle Holocene age (swamp and lagoon facies associations) include stacked peat layers and fossiliferous horizons with a high correlation potential, formed in inner-estuarine to delta-plain environments (Amorosi *et al.*, 2017a; Bruno *et al.*, 2017b, 2019). Two well identifiable lagoon horizons (M4 in Fig. 4 and M5 in Fig. 5), 1 to 3 m thick, were selected as Holocene marker beds. These key stratigraphic horizons are typified by a distinctive brackish meiofauna and appear to be tilted and/or folded in the Argenta–Longastrino area (Fig. 1), with differences in elevation up to 10 m (Figs 4 and 5).

Stratigraphic markers M4 and M5 record a marked lateral facies variability, with distinct changes in lithofacies characteristics and fossil associations. They provide, in particular, robust signals of brackish sub-environments in a microtidal (<1 m) setting (see previous section). Therefore, they represent excellent indicators of the mean sea-level (with an uncertainty of 2 m – Scarponi *et al.*, 2013). Due to their limited thickness, they approximate almost perfect horizontal surfaces at the time of deposition. Marker beds M4 and M5 yielded consistent calibrated ages of 8.6 to 8.3 kyr BP (M4) and 6.2 to 5.6 kyr BP (M5), respectively, from basal peats, wood and shell samples.

SEISMIC STRATIGRAPHY

Detailed reconstruction of deep stratal architecture in the study area was carried out through the interpretation of 95 two-dimensional seismic profiles from the ENI s.p.a. database, after calibration with 45 well logs available online at <https://unmig.mise.gov.it/>. Analysis and interpretation of seismic profiles focused on the identification of major angular unconformities and their correlative conformities (Vail *et al.*, 1997).

The main tectonic structures in the subsurface of the Po Plain are well imaged by seismic lines with SSW–NNE orientation, i.e. perpendicular to the strike of major thrusts and anticlines (Fig. 7A). Three basin-scale unconformity-bounded units were identified and classified, based on their geometry and on seismic-reflector terminations: (i) a basal pre-tectonic unit showing parallel seismic reflectors, faulted and folded in the hangingwall; (ii) an intermediate, highly deformed and wedge-shaped syntectonic unit, with seismic reflectors converging towards the culmination of thrust-related anticlines; and (iii) an upper unit with basin-wide occurrence, draping the whole succession and sealing the buried thrust fronts (Picotti & Pazzaglia, 2008 – Fig. 7A). Based on palaeontological (foraminifera and nannoplankton) data available from well-log descriptions, the unconformities that separate these units were assigned to the Messinian and Early Pleistocene (Calabrian), respectively.

According to the ENI stratigraphy (Ghielmi *et al.*, 2013; Amadori *et al.*, 2019), the ‘post-tectonic’ unit includes two formations (Fig. 7): Carola Formation, of Early Pleistocene age, and Ravenna Formation, of Middle Pleistocene–Holocene age. Within the Ravenna Formation, two unconformities, identified on the basis of well log correlation and dated approximately to 0.87 Myr and 0.4 Myr (Regione Emilia-Romagna & ENI-AGIP, 1998), respectively, mark the lower boundaries of two minor unconformity-bounded stratigraphic units: Lower Po Synthem and Upper Po Synthem (Amorosi *et al.*, 2008 – Fig. 7A), also referred to as ‘AEI’ and ‘AES’ (Regione Emilia-Romagna & ENI-AGIP, 1998) in the Geological Map of Italy to 1 : 50 000 scale. The reader is referred to these studies for detailed description of such units.

Cross-sectional stratal geometries and seismic reflection terminations were used to isolate stratal discontinuities in the study area. Near-horizontal reflectors with planar onlap terminations onto the

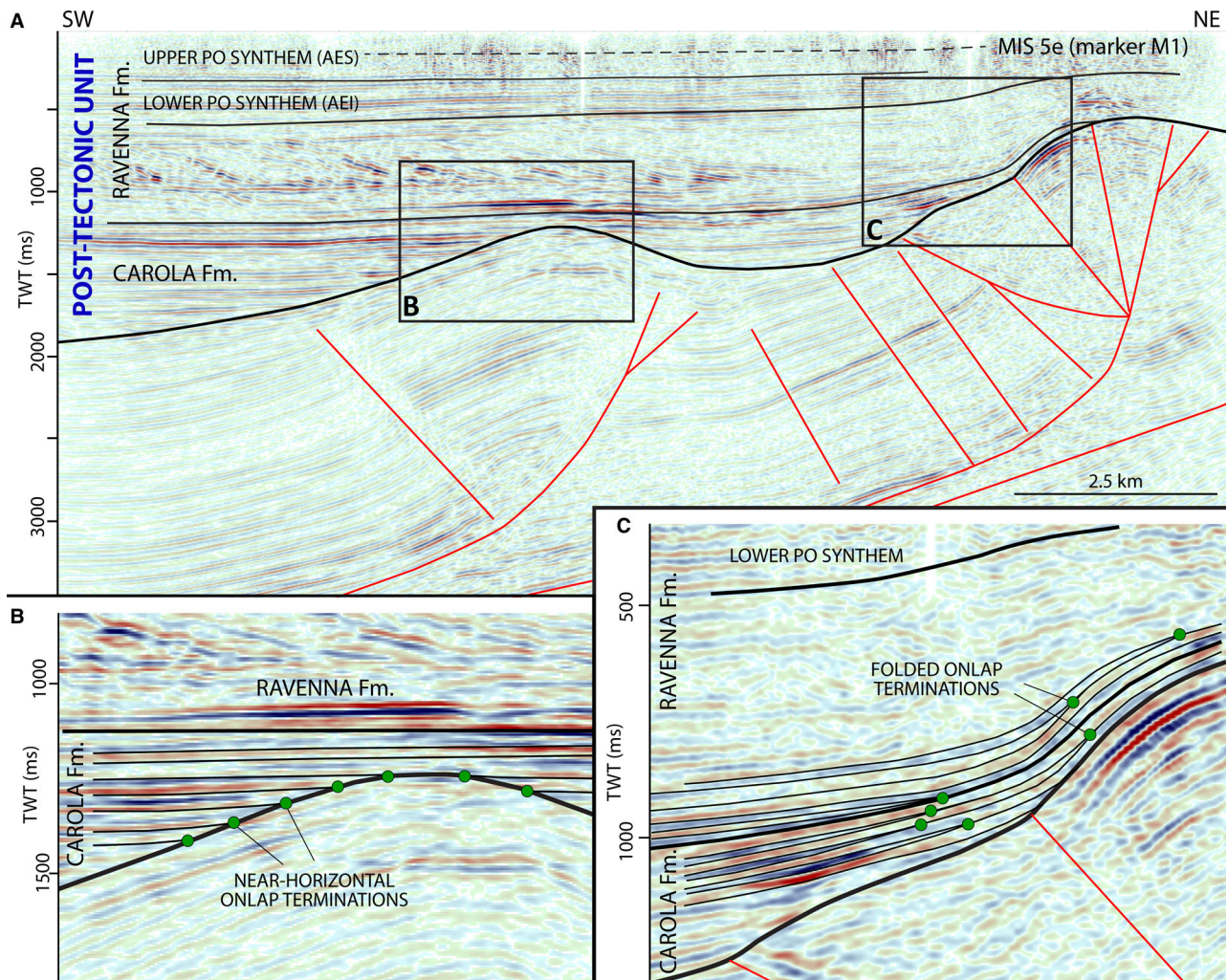


Fig. 7. Interpreted seismic profile in the Longastrino area (section trace in Fig. 1), showing major tectonic structures and stratal geometries across the Po basin fill. (A) Seismic stratigraphy of the presumed 'post-tectonic' unit. (B) Near-horizontal onlap terminations of the Carola Formation onto the highly deformed Miocene substrate. (C) Onlap terminations folded into a gentle anticline and tilted by the growth of the active thrust front. TWT = two-way travelttime.

lower bounding unconformity are recurrent features in the Carola Formation, at relatively southern locations (Fig. 7B). In contrast, south-west of the structural culminations, onlapping reflectors of the upper Carola and Ravenna formations show distinctive inclined geometries, suggesting that they were tilted by the growth of the Longastrino anticline (Fig. 7C). Seismic resolution decreases dramatically in the upper Ravenna formation, where the stratigraphic discontinuity at the base of the Lower Po synthem is gently deformed, whereas the base of the Upper Po Synthem seemingly appears as an undisturbed flat surface and can hardly be tracked onto the structural high (Fig. 7A).

CAN FOLDING OF BURIED STRATIGRAPHIC MARKERS REVEAL *LOCI* OF ACTIVE TECTONIC DEFORMATION?

Robust evidence of folding of laterally extensive key horizons M1 to M5 from the subsurface of the Po Plain enables the reconstruction of a coherent, high-resolution record of Last Interglacial to Recent deformation at the sub-seismic scale, focused in the Argenta-Longastrino area (Figs 1, 4 and 5). To test for possible links between shallow deformation of stratigraphic markers M1 to M5 and active tectonics in the area, the stratigraphic cross-sections of Figs 4

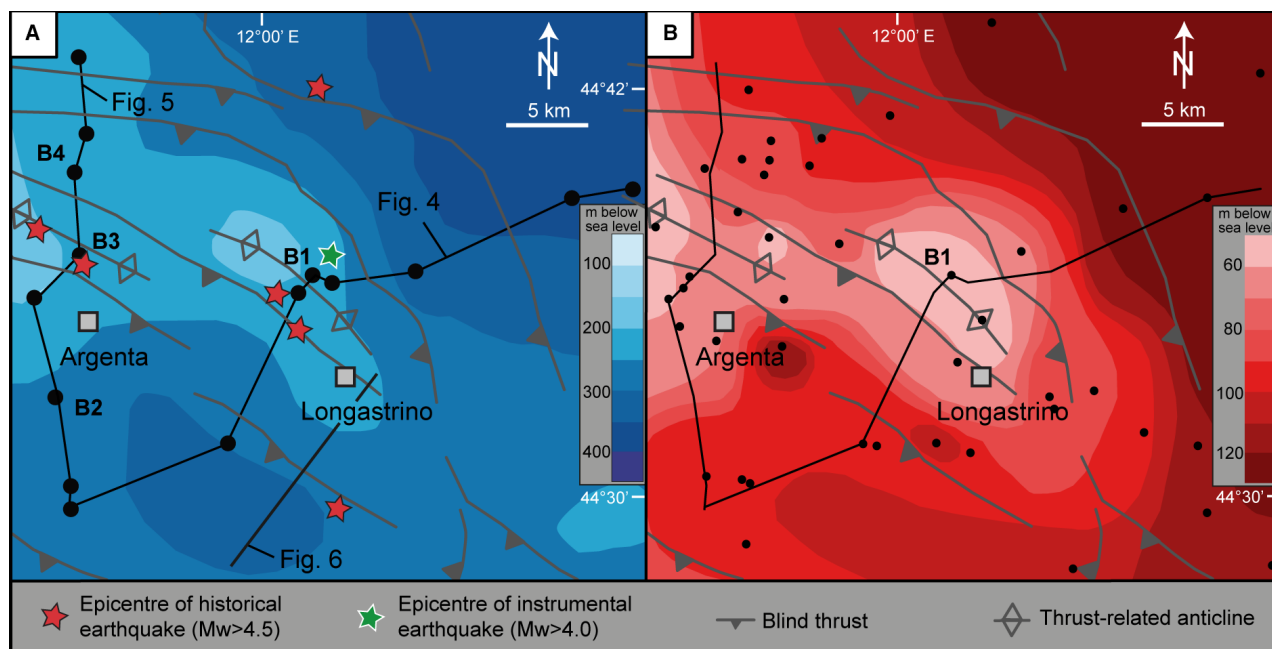


Fig. 8. Subsurface geology of the study area: (A) Depth map of the Lower/Upper Po Synthem boundary (0.4 Myr unconformity – from Martelli *et al.*, 2017) and the earthquake catalogue of Fig. 1A. (B) Contour map of the top of Marker M1 (125 kyr – MIS 5e – coastal sand body); dots represent the stratigraphic dataset. The areas where antiformal geometries of marker horizons M2 to M5 are best observed, around cores B1 (Fig. 4) and B3 (Fig. 5), coincide spatially with the same structural culmination north of Argenta and Longastrino.

and 5 were plotted against the depth map of the boundary between Lower and Upper Po Synthems (AEI/AES boundary in the Geological Map of Italy – Fig. 8A). This stratigraphic discontinuity, which is not clearly imaged on seismic profiles (Fig. 7A), represents the youngest (*ca* 0.4 Myr) deformed horizon mapped in the eastern Po Basin, so far (Martelli *et al.*, 2017). In order to emphasize the use of facies analysis and high-resolution stratigraphy as an aid in the recognition of deformation patterns, a map of the depth of top marker M1 was also constructed (Fig. 8B).

The spatial overlap between: (i) the deformation of the 0.4 Myr unconformity (Fig. 8A); (ii) the deformation of top marker M1 (Fig. 8B); (iii) the anticline culminations of markers M2 to M5 (Figs 4 and 5); and (iv) earthquake locations (Fig. 8A) is apparent and provides some support for the hypothesis that part of the folding affecting the sedimentary units along the Argenta–Longastrino ridge could be the result of earthquakes. Historic sources indicate that earthquakes took place in the Po Plain along the Ferrara–Romagna arc since the Roman Period (Stefani *et al.*, 2018). The surface distribution of

historical earthquakes points to clustered seismicity around the Mirandola, Ferrara, Argenta and Longastrino ridges (Figs 1A and 8A). Apart from the two major events in the epicentral area of the 2012 seismic sequence (close to Mirandola), historical and instrumental catalogues report 20 earthquakes with $M_w > 4.5$ (Table S2), but earthquakes greater than magnitude 5 are rare in the region (Fig. 1A). Historical data indicate that the nearest recent notable earthquakes occurred near Ferrara ($M_w = 5.44$) and Argenta ($M_w = 5.43$ – Fig. 8A). These earthquakes date back to 1570 and 1624, respectively. The focal mechanisms of all instrumental events associated with the Ferrara arc show prevalent reverse and reverse-oblique kinematics, with P-axes nearly perpendicular to the average structural trend (Lavecchia *et al.*, 2012).

The deformation of marker horizons M1 to M5 in the Argenta–Longastrino region (Figs 4 and 5) is remarkably coincident with the axis of the buried ramp anticline (Figs 7A and 8). Punctuated co-seismic activity was likely followed by post-seismic relaxation and prolonged periods of inter-seismic locking, during which sedimentation overwhelmed tectonics (Carminati *et al.*,

2010), restoring flat topographic conditions in the alluvial plain (Bruno *et al.*, 2019). However, the deformation inferred from stratigraphic analysis might reflect complex interplay of slip along the buried thrust and associated ramp anticline uplift, as well as differential sediment compaction and loading. Since the anticlinal culmination pre-dates the studied succession, the deformation could have been enhanced by sediment compaction in the syncline successions, where highly compressible, swamp (peat-rich) deposits are thicker (Fig. 5).

Partitioning precisely the entire deformation budget into its components: (i) tectonics, i.e. uplift of the anticline crest and foreland subsidence; and (ii) compaction, i.e. subsidence due to porosity reduction, is problematic and largely beyond the scope of this paper (see Scrocca *et al.*, 2007, and Bresciani & Perotti, 2014, for reconstruction of relative uplift rates from the adjacent Mirandola and other Po Plain buried anticlines). Comparing the geometry of marker horizon M1 with that of M2 to M5 markers could help with separating the relative effects of subsidence and anticline crest uplift, although reliable quantification would require a larger dataset.

In summary, several lines of evidence from different fields (core stratigraphy, seismic stratigraphy, structural geology and seismology) suggest that folding of laterally continuous stratigraphic markers across the Argenta–Longastrino ridge could be, in part at least, the manifestation of active tectonic deformation. Supporting evidence for tectonically induced deformation can be summarized, as follows:

1 The areas where MIS 5e to MIS 1 stratigraphic markers exhibit clear antiformal geometries (Figs 4 and 5) are strikingly coincident with the epicentres of historic and instrumental seismicity dating back to the last five centuries (Fig. 8A).

2 Deformation of marker horizons M1 to M5 across the Argenta–Longastrino ridge (Figs 4 and 5) shows strong correspondence with the location of major thrust fronts inferred independently from prior geophysical investigations (Figs 1 and 8).

3 Thrust-related folding of Middle Pleistocene–Holocene marker beds M1 to M5 coincides spatially with the deformation of Lower Pleistocene seismic onlap terminations that elsewhere in the basin exhibit typical near-horizonal geometries (Fig. 7).

Although precise 3D control on facies architecture is not available, the spatial distribution of depositional systems outlined in this work (Figs 4 and 5) also suggests a strong influence of the underlying tectonic structures on sedimentation. Beach-barrier systems, for example, are abruptly replaced landward (to the south-west) by unusually thick lagoon deposits, just above the Longastrino ridge (Fig. 4). This stratigraphic configuration suggests a morphological (possibly tectonic) control on the Early Holocene (south-west-directed) shoreline retrogradation and subsequent (north-east-directed) progradation. A similar control could be envisaged for Upper Pleistocene swamp/poorly-drained floodplain deposits sandwiched between alluvial facies (Fig. 5): the remarkably lenticular geometry of this wetland depositional system, which thickens in the syncline and wedges out onto the structural high, suggests that paludal environments occupied the lowest position in the landscape, as an effect of a possibly growing, active structure to the south-west.

Further progress is required to constrain the spatial distribution of syndepositional deformation. There is a need, in particular, for comprehensive subsurface mapping of the most prominent stratigraphic markers (M2 to M5).

Beyond the Po Plain, the facies-based approach shown in this paper appears to be broadly applicable to upper Quaternary alluvial, deltaic and coastal systems from other active tectonic regions, where the contribution of high-resolution stratigraphic studies to unravel tectonic deformation has been neglected. In particular, tracking deformation across Upper Pleistocene–Holocene sediment packages on a millennial timescale can bridge the gap between the analysis of long-term (basin-scale), steady-state tectonics acting on 10^5 to 10^7 year time periods, and short-term (fault-controlled) deformation primarily developed on 10^0 to 10^2 year timescales.

SUMMARY AND OUTLOOK

Assessing the seismogenic potential of fault systems beneath alluvial and coastal plains is commonly hindered, especially in actively subsiding basins, by the lack of surface signatures and topographic relief. In such areas, where active tectonics has a poor geomorphic expression and thick Quaternary sedimentary covers preclude calculations of uplift rates, only loosely constrained

inferences on the surface propagation of tectonic deformation are generally available.

This paper has shown that high-resolution core-based stratigraphy in the ^{14}C , optically stimulated luminescence (OSL) and electron spin resonance (ESR) time windows, used in conjunction with conventional seismic stratigraphy can represent a powerful tool to assess a decipherable record of near-surface tectonic deformation. The notable deformation of the Last Interglacial (MIS 5e) nearshore sand body and of a series of prominent stratigraphic markers of Late Pleistocene–Holocene age across structural lineaments of the southern Po Plain correlates closely with seismic observations and historic/instrumental earthquake data. Detailed analysis of seismic-reflector terminations from the Carola Formation shows clear evidence of syn-tectonic deformation (onlap deformation, decreasing thickness and converging reflectors towards growing anticlines) close to targeted faults. In general, Quaternary deformation is clearly reproducing the general pattern of bed-rock folds.

Stratigraphic markers of distinct ages and belonging to different facies associations, were examined: (i) beach-barrier deposits (marker M1) dated to MIS 5e (about 125 kyr BP); (ii) two Upper Pleistocene palaeosols (markers M2 and M3), assigned to the MIS 3/2 transition (29 to 24 cal kyr BP), and to the Younger Dryas cold spell (13 to 11 cal kyr BP), respectively; and (iii) two Holocene lagoon horizons (M4 and M5), dated to 8.6 to 8.3 cal kyr BP and 6.2 to 5.6 cal kyr BP, respectively.

Beach-barrier and lagoon/outer estuary horizons are the most sensitive indicators of post-burial deformation, because they represent approximately horizontal surfaces at the time of deposition that can be delineated objectively over large portions of the basin. Brackish deposits, in particular, can be easily ascertained on the basis of refined palaeontological criteria and readily differentiated from adjacent freshwater (swamp/inner estuary) and coastal deposits.

The subsurface stratigraphic approach set out in this study, based on a strongly constrained chronological framework, is widely applicable to Upper Pleistocene and Holocene successions of densely populated lowlands worldwide, where the record of past seismic events is no longer prominent in the flat morphology. In such regions, reconstructing the shallow stratigraphy through a combined sedimentological and palaeoecological analysis can delineate areas of

possible active tectonic deformation beyond the limits of geomorphological and palaeoseismic records.

ACKNOWLEDGEMENTS

This study was partially supported by the Basic Research Project of the Korean Institute of Geoscience and Mineral Resources (KIGAM) funded by the Ministry of Science and ICT of Korea. The authors declare that there is no conflict of interest. We thank Associate Editor Adam McArthur, Martin Muravchik and an anonymous reviewer for their constructive and insightful comments.

DATA AVAILABILITY STATEMENT

The data that support the findings of this study are available in the supplementary material of this article.

REFERENCES

- Aitken, M.J. (1985) *Thermoluminescence Dating*. Orlando, FL: Academic Press.
- Amadori, C., Toscani, G., Di Giulio, A., Maesano, F.E., D'Ambrogio, C., Ghielmi, M. and Fantoni, R. (2019) From cylindrical to non-cylindrical foreland basin: Pliocene–Pleistocene evolution of the Po Plain–Northern Adriatic basin (Italy). *Basin Res.*, **31**, 991–1015.
- Amorosi, A. and Marchi, N. (1999) High-resolution sequence stratigraphy from piezocone tests: an example from the Late Quaternary deposits of the SE Po Plain. *Sed. Geol.*, **128**, 69–83.
- Amorosi, A., Centineo, M.C., Colalongo, M.L., Pasini, G., Sarti, G. and Vaiani, S.C. (2003) Facies architecture and Latest Pleistocene–Holocene depositional history of the Po Delta (Comacchio area), Italy. *J. Geol.*, **111**, 39–56.
- Amorosi, A., Colalongo, M.L., Fiorini, F., Fusco, F., Pasini, G., Vaiani, S.C. and Sarti, G. (2004) Palaeogeographic and palaeoclimatic evolution of the Po Plain from 150-ky core records. *Global Planet. Change*, **40**, 55–78.
- Amorosi, A., Centineo, M.C., Colalongo, M.L. and Fiorini, F. (2005) Millennial-scale depositional cycles from the Holocene of the Po Plain, Italy. *Mar. Geol.*, **222–223**, 7–18.
- Amorosi, A., Pavesi, M., Ricci Lucchi, M., Sarti, G. and Piccin, A. (2008) Climatic signature of cyclic fluvial architecture from the Quaternary of the central Po plain, Italy. *Sed. Geol.*, **209**, 58–68.
- Amorosi, A., Bruno, L., Campo, B. and Morelli, A. (2015) The value of pocket penetration tests for the high-resolution palaeosol stratigraphy of late Quaternary deposits. *Geol. J.*, **50**, 670–682.
- Amorosi, A., Bruno, L., Campo, B., Morelli, A., Rossi, V., Scarponi, D., Hong, W., Bohacs, K.M. and Drexler, T.M. (2017a) Global sea-level control on local parasequence

- architecture from the Holocene record of the Po Plain, Italy. *Mar. Petrol. Geol.*, **87**, 99–111.
- Amorosi, A., Bruno, L., Cleveland, D.M., Morelli, A. and Hong, W.** (2017b) Paleosols and associated channel-belt sand bodies from a continuously subsiding late Quaternary system (Po Basin, Italy): new insights into continental sequence stratigraphy. *Geol. Soc. Am. Bull.*, **129**, 449–463.
- Amorosi, A., Barbieri, G., Bruno, L., Campo, B., Drexler, T.M., Hong, W., Rossi, V., Sammartino, I., Scarponi, D., Vaiani, S.C. and Bohacs, K.M.** (2019) Three-fold nature of coastal progradation during the Holocene eustatic highstand, Po Plain, Italy—close correspondence of stratal character with distribution patterns. *Sedimentology*, **66**, 3029–3052.
- Amorosi, A., Bruno, L., Campo, B., Costagli, B., Dinelli, E., Sammartino, I. and Vaiani, S.C.** (2020) Tracing clinothem geometry and sediment pathways in the prograding Holocene Po Delta system through integrated core stratigraphy. *Basin Res.*, **32**, 206–215.
- Audemard, F.A. and Michetti, A.M.** (2011) Geologic criteria for evaluating seismicity revisited: forty years of paleoseismic investigations and the natural record of past earthquakes. In: *Geologic Criteria for Evaluating Seismicity Revisited: Forty Years of Paleoseismic Investigations and the Natural Record of Past Earthquakes* (Eds Audemard, F.A., Michetti, A.M. and McCalpin, J.P.), *Geol. Soc. Am. Sp. Paper*, **479**, 1–22. Boulder, CO.
- Azor, A., Keller, E.A. and Robert, S.Y.** (2002) Geomorphic indicators of active fold growth: South Mountain-Oak Ridge anticline, Ventura basin, southern California. *Geol. Soc. Am. Bull.*, **114**, 745–753.
- Barbieri, G. and Vaiani, S.C.** (2018) Benthic foraminifera or Ostracoda? Comparing the accuracy of palaeoenvironmental indicators from a Pleistocene lagoon of the Romagna coastal plain (Italy). *J. Micropaleontology*, **37**, 203–230.
- Barbieri, G., Rossi, V., Vaiani, S.C. and Horton, B.P.** (2019) Benthic ostracoda and foraminifera from the North Adriatic Sea (Italy, Mediterranean Sea): a proxy for the depositional characterisation of river-influenced shelves. *Mar. Micropaleontology*, **153**, 101772.
- Barka, A., Akyüz, A., Altunel, H.S., Sunal, G., Çakir, Z., Dikbaş, A., Yeli, B., Armijo, R., Meyer, B., de Chabaliér, J.B., Rockwell, T., Dolan, J.R., Hartleb, R., Dawson, T., Christoferson, S., Tucker, A., Fumal, T., Langridge, R., Stenner, H., Lettis, W., Bachhuber, J. and Page, W.** (2002) The surface rupture and slip distribution of the 17 August 1999 Izmit earthquake (M 7.4), North Anatolian Fault. *Bull. Seismol. Soc. Am.*, **92**, 43–60.
- Begg, J.G., Mildenhall, D.C., Lyon, G.L., Stephenson, W.R., Funnell, R.H. and Van Dissen, R.J.** (1993) A paleoenvironmental study of subsurface Quaternary sediments at Wainuiomata, Wellington, New Zealand, and tectonic implications. *NZ J. Geol. Geophys.*, **36**, 461–473.
- Bhattacharya, J.P. and MacEachern, J.A.** (2009) Hyperpycnal rivers and prodeltaic shelves in the Cretaceous Seaway of North America. *J. Sed. Res.*, **79**, 184–209.
- Boccalletti, M., Corti, G. and Martelli, L.** (2011) Recent and active tectonics of the external zone of the Northern Apennines (Italy). *Int. J. Earth Sci.*, **100**, 1331–1348.
- Bohacs, K.M., Lazar, O.R. and Demko, T.M.** (2014) Parasequence types in shelfal mudstone strata—Quantitative observations of lithofacies and stacking patterns, and conceptual link to modern depositional regimes. *Geology*, **42**, 131–134.
- Bonini, L., Toscani, G. and Seno, S.** (2014) Three-dimensional segmentation and different rupture behavior during the 2012 Emilia seismic sequence (Northern Italy). *Tectonophysics*, **630**, 33–42.
- Bresciani, I. and Perotti, C.R.** (2014) An active deformation structure in the Po Plain (N Italy): the Romanengo anticline. *Tectonics*, **33**, 2059–2076.
- Bronk Ramsey, C.** (2009) Dealing with outliers and offsets in radiocarbon dating. *Radiocarbon*, **51**, 1023–1045.
- Bruno, L., Amorosi, A., Severi, P. and Costagli, B.** (2017a) Late Quaternary aggradation rates and stratigraphic architecture of the southern Po Plain, Italy. *Basin Res.*, **29**, 234–248.
- Bruno, L., Bohacs, K.M., Campo, B., Drexler, T.M., Rossi, V., Sammartino, I., Scarponi, D., Hong, W. and Amorosi, A.** (2017b) Early Holocene transgressive palaeogeography in the Po coastal plain (northern Italy). *Sedimentology*, **64**, 1792–1816.
- Bruno, L., Campo, B., Di Martino, A., Hong, W. and Amorosi, A.** (2019) Peat layer accumulation and post-burial deformation during the mid-late Holocene in the Po coastal plain (Northern Italy). *Basin Res.*, **31**, 621–639.
- Bruno, L., Marchi, M., Bertolini, I., Gottardi, G. and Amorosi, A.** (2020) Climate control on stacked paleosols in the Pleistocene of the Po Basin (northern Italy). *J. Quatern. Sci.*, **35**, 559–571.
- Campo, B., Amorosi, A. and Vaiani, S.C.** (2017) Sequence stratigraphy and late Quaternary paleoenvironmental evolution of the Northern Adriatic coastal plain (Italy). *Palaeogeogr. Palaeoclimatol. Palaeoecol.*, **466**, 265–278.
- Campo, B., Bohacs, K.M. and Amorosi, A.** (2020a) Late Quaternary sequence stratigraphy as a tool for groundwater exploration: lessons from the Po River Basin (northern Italy). *AAPG Bull.*, **104**, 681–710.
- Campo, B., Bruno, L. and Amorosi, A.** (2020b) Basin-scale stratigraphic correlation of Late Pleistocene-Holocene (MIS 5e-MIS 1) strata across the rapidly subsiding Po Basin (northern Italy). *Quatern. Sci. Rev.*, **237**, 106300.
- Caputo, R., Pellegrinelli, A., Bignami, C., Bondesan, A., Mantovani, A., Stramondo, S. and Russo, P.** (2015) High-precision levelling, DInSAR and geomorphological effects in the Emilia 2012 epicentral area. *Geomorphology*, **235**, 106–117.
- Carannante, S., Argnani, A., Massa, M., D'Alema, E., Lovati, S., Moretti, M., Cattaneo, M. and Augliera, P.** (2015) The May 20 (Mw 6.1) and 29 (Mw 6.0), 2012, Emilia (Po Plain, northern Italy) earthquakes: new seismotectonic implications from subsurface geology and high-quality hypocenter location. *Tectonophysics*, **655**, 107–123.
- Carminati, E., Martinelli, G. and Severi, P.** (2003) Influence of glacial cycles and tectonics on natural subsidence in the Po Plain (northern Italy): Insights from ^{14}C ages. *Geochem. Geophys. Geosyst.*, **4**, <https://doi.org/10.1029/2002GC000481>
- Carminati, E., Scrocca, D. and Doglioni, C.** (2010) Compaction-induced stress variations with depth in an active anticline: Northern Apennines, Italy. *J. Geophys. Res. Solid Earth*, **115**, <https://doi.org/10.1029/2009JB006395>.
- Dasgupta, U., Barbieri, G., Vaiani, S.C. and Ghosh, A.** (2020) Potential and limits of benthic foraminiferal ecological indices in paleoenvironmental reconstructions: a case from a Holocene succession of the Po Delta, Italy. *Micropaleontology*, **66**, 103–126.

- Debenay, J.P. and Guillou, J.J. (2002) Ecological transitions indicated by foraminiferal assemblages in paralic environments. *Estuaries Coasts*, **25**, 1107–1120.
- Debenay, J.P., Guillou, J.J., Redois, F. and Geslin, E. (2000) Distribution trends of foraminiferal assemblages in paralic environments: a base for using foraminifera as bioindicators. In: *Environmental Micropaleontology: The Application of Microfossils to Environmental Geology* (Ed. Martin, R.E.), pp. 39–67. Kluwer Academic/Plenum Publishers, New York.
- DISS Working Group (2018) Database of individual seismogenic sources (DISS), version 3.2.0: A compilation of potential sources for earthquakes larger than M 5.5 in Italy and surrounding areas. Istituto Nazionale di Geofisica e Vulcanologia. <https://doi.org/10.6092/INGV.IT-DISS3.2.0>. Available at: <http://diss.rm.ingv.it/diss/>
- Dogliani, C. (1993) Some remarks on the origin of foredeeps. *Tectonophysics*, **228**, 1–20.
- Dura, T., Hemphill-Haley, E., Saway, Y. and Horton, B.P. (2016) The application of diatoms to reconstruct the history of subduction zone earthquakes and tsunamis. *Earth Sci. Rev.*, **152**, 181–197.
- Durcan, J.A., King, G.E. and Duller, G.A.T. (2015) DRAC: Dose rate and age calculator for trapped charge dating. *Quatern. Geochron.*, **28**, 54–61.
- Fantoni, R. and Franciosi, R. (2010) Tectono-sedimentary setting of the Po Plain and Adriatic foreland. *Rend. Fis. Acc. Lincei*, **21**(1), S197–S209.
- Ferranti, L., Antonioli, F., Mauz, B., Amorosi, A., Dai Pra, G., Mastronuzzi, G., Monaco, C., Orrù, P., Pappalardo, M., Radtke, U., Renda, P., Romano, P., Sansò, P. and Verrubbi, V. (2006) Markers of the last interglacial sea-level high stand along the coast of Italy: Tectonic implications. *Quatern. Int.*, **145–146**, 30–54.
- Garzanti, E., Vezzoli, G. and Andò, S. (2011) Paleogeographic and paleodrainage changes during Pleistocene glaciations (Po Plain, Northern Italy). *Earth Sci. Rev.*, **105**, 25–48.
- Geological Map of Italy at 1:50,000 scale (Geological Survey of Italy and CARG Project). Available at: <http://www.ispraambiente.gov.it/Media/carg/emilia.html>
- Ghielmi, M., Minervini, M., Nini, C., Rogledi, S., Rossi, M. and Vignolo, A. (2010) Sedimentary and tectonic evolution in the eastern Po Plain and northern Adriatic Sea area from Messinian to Middle Pleistocene (Italy). *Rend. Fis. Acc. Lincei*, **21**, 131–166.
- Ghielmi, M., Minervini, M., Nini, C., Rogledi, S. and Rossi, M. (2013) Late Miocene-Middle Pleistocene sequences in the Po Plain-Northern Adriatic Sea (Italy): the stratigraphic record of modification phases affecting a complex foreland basin. *Mar. Petrol. Geol.*, **42**, 50–81.
- Goineau, A., Fontanier, C., Jorissen, F.J., Lansard, B., Buscail, R., Mouret, A., Kerhervé, P., Zaragosi, S., Ernoul, E., Artéro, C., Anschutz, P., Metzger, E. and Rabouille, C. (2011) Live (stained) benthic foraminifera from the Rhône prodelta (Gulf of Lion, NW Mediterranean): Environmental controls on a river-dominated shelf. *J. Sea Res.*, **65**, 58–75.
- Govoni, A., Marchetti, A., De Gori, P., Di Bona, M., Lucente, F.P., Improta, L., Chiarabba, C., Nardi, A., Margheriti, L., Piana Agostinetti, N., Di Giovambattista, R., Latorre, D., Anselmi, M., Ciaccio, M.G., Moretti, M., Castellano, C. and Piccinini, D. (2014) The 2012 Emilia seismic sequence (Northern Italy): Imaging the thrust fault system by accurate aftershock location. *Tectonophysics*, **622**, 44–55.
- Guccione, M.J., Burford, M.F. and Kendall, J.D. (2009) Pemiscot Bayou, a large distributary of the Mississippi River and a possible failed avulsion. In: *Fluvial Sedimentology VI* (Eds Smith, N.D. and Rogers, J.), *Int. Assoc. Sedimentol. Sp. Publ.*, **28**, 211–220. Blackwell Science, Oxford and Northampton.
- Gunderson, K.L., Anastasio, D.J., Pazzaglia, F.J. and Kodama, K.P. (2018) Intrinsically variable blind thrust faulting. *Tectonics*, **37**, 1454–1471.
- Guerin, G., Mercier, N. and Adamiec, G. (2011) Dose-rate conversion factors. *Ancient TL*, **29**, 5–8.
- Helmens, K.F. (2014) The Last Interglacial-Glacial cycle (MIS 5–2) re-examined based on long proxy records from central and northern Europe. *Quatern. Sci. Rev.*, **86**, 115–143.
- Hobday, D.K. (1978) Fluvial deposits of the Ecca and Beaufort Groups in the Eastern Karoo Basin, Southern Africa. In: *Fluvial Sedimentology* (Ed. Miall, A.D.), *Can. Soc. Petrol. Geol. Mem.*, **5**, 413–430.
- Ishiyama, T., Mueller, K., Sato, H. and Togo, M. (2007) Coseismic fault-related fold model, growth structure, and the historic multisegment blind thrust earthquake on the basement-involved Yoro thrust, central Japan. *J. Geophys. Res.*, **112**, B03S07.
- Ishiyama, T., Sato, H., Kato, N., Nakayama, T. and Abe, S. (2013) Active blind thrusts beneath the Tokyo metropolitan area: seismic hazards and inversion tectonics. *Geophys. Res. Lett.*, **40**, 2608–2612.
- ISIDE Working Group (2015) Italian Seismological Instrumental and parametric Data-base. Istituto Nazionale di Geofisica e Vulcanologia. Available at: <http://cnt.rm.ingv.it/en/iside>
- Jorissen, F.J. (1988) Benthic Foraminifera from the Adriatic Sea; principles of phenotypic variation. *Utrecht Micropaleontol. Bull.*, **37**, 1–176.
- Jorissen, F.J., Nardelli, M.P., Almogi-Labin, A., Barras, C., Bergamin, L., Bicchì, E., El Kateb, A., Ferraro, L., McGann, M., Morigi, C., Romano, E., Sabbatini, A., Schweizer, M. and Spezzaferri, S. (2018) Developing Foram-AMBI for biomonitoring in the Mediterranean: species assignments to ecological categories. *Mar. Micropaleontol.*, **140**, 33–45.
- Keller, E.A. and Pinter, N. (2002) *Active Tectonics: Earthquakes, Uplift, and Landscape*, 2nd edn. Prentice Hall, Upper Saddle River, NJ.
- Kraus, M.J. and Aslan, A. (1993) Eocene hydromorphic paleosols: Significance for interpreting ancient floodplain processes. *J. Sed. Petrol.*, **63**, 453–463.
- Lavecchia, G., de Nardis, R., Cirillo, D., Brozzetti, F. and Boncio, P. (2012) The May-June 2012 Ferrara Arc earthquakes (northern Italy): structural control of the spatial evolution of the seismic sequence and of the surface pattern of coseismic fractures. *Ann. Geophys.*, **55**, 533–540.
- Livani, M., Scrocca, D., Arecco, P. and Dogliani, C. (2018) Structural and stratigraphic control on salient and recess development along a thrust belt front: The Northern Apennines (Po Plain, Italy). *J. Geophys. Res. Solid Earth*, **123**, 4360–4387.
- Livio, F., Michetti, A.M., Ticozzi, E. and Porfido, S. (2014) The ESI macroseismic field for the 1624 AD Argenta earthquake (Po Plain – N Italy): an integrated macroseismic approach to overcome MCS misfitting. *Rend. Soc. Geol. Ital.*, **31**, <https://doi.org/10.3301/ROL.2014.140>
- Maesano, F.E., D'Ambrogi, C., Burrato, P. and Toscani, G. (2015) Slip-rates of blind thrusts in slow deforming areas:

- examples from the Po Plain (Italy). *Tectonophysics*, **643**, 8–25.
- Malinverno, A. and Ryan, W.B.F.** (1986) Extension in the Tyrrhenian Sea and shortening in the Apennines as result of arc migration driven by sinking of the lithosphere. *Tectonics*, **5**, 227–245.
- Martelli, L., Bonini, M., Calabrese, L., Corti, G., Ercolessi, G., Molinari, F.C., Piccardi, L., Pondrelli, S., Sani, F. and Severi, P.** (2017) *Seismotectonic map of the Emilia-Romagna Region and surrounding areas, Scale 1:250,000*, 2nd edn. D.R.E.A.M., Firenze.
- Matsu'ura, T. and Sugaya, K.** (2017) Late Quaternary crustal shortening rates across thrust systems beneath the Ou Ranges in the NE Japan arc inferred from fluvial terrace deformation. *J. Asian Earth Sci.*, **140**, 13–30.
- Morelli, A., Bruno, L., Cleveland, D.M., Drexler, T.M. and Amorosi, A.** (2017) Reconstructing Last Glacial Maximum and Younger Dryas paleolandscapes through subsurface paleosol stratigraphy: An example from the Po coastal plain, Italy. *Geomorphology*, **295**, 790–800.
- Murray, J.W.** (2006) *Ecology and Applications of Benthic Foraminifera*. Cambridge University Press, Cambridge.
- Muttoni, G., Carcano, C., Garzanti, E., Ghielmi, M., Piccin, A., Pini, R., Rogledi, S. and Sciunnach, D.** (2003) Onset of major Pleistocene glaciations in the Alps. *Geology*, **31**, 989–992.
- Niwa, Y., Sugai, T., Matsushima, Y. and Toda, S.** (2019) Millennial-scale crustal movements inferred from Holocene sedimentary succession of the Omoto plain, northern Sanriku coast, Northeast Japan: Relevance for modeling megathrust earthquake cycles. *Mar. Geol.*, **519**, 10–24.
- Niwa, Y. and Sugai, T.** (2020) An assessment of coastal tectonics along the Sanriku coast, northeast Japan, from a Holocene sedimentary succession in the Kuji plain. *Mar Geol.*, **424**, 106165.
- O'Leary, M.J., Hearty, P.J., Thompson, W.G., Raymo, M.E., Mitrovica, J.X. and Webster, J.M.** (2013) Ice-sheet collapse following a prolonged period of stable sea level during the last interglacial. *Nat. Geosci.*, **6**, 796–800.
- Picotti, V., Capozzi, R., Bertozzi, G., Mosca, F., Sitta, A. and Tornaghi, M.** (2007) The Miocene petroleum system of the Northern Apennines in the central Po Plain (Italy). In: *Thrust belts and foreland basins. From fold Kinematics to Hydrocarbon Systems* (Eds Lacombe, O., Lavé, J., Roure, F. and Vergés, J.), pp. 117–131. Springer Verlag, Berlin.
- Picotti, V. and Pazzaglia, F.J.** (2008) A new active tectonic model for the construction of the Northern Apennines mountain front near Bologna (Italy). *J. Geophys. Res.*, **113**, B08412.
- Pieri, M. and Groppi, G.** (1981) Subsurface geological structure of the Po Plain, Italy. In: *Progetto Finalizzato Geodinamica* (Eds Pieri, M. and Groppi, G.), 414th edn, pp. 1–23. C.N.R., Roma, Italy.
- Prentice, C.S., Mann, P., Crone, A.J., Gold, R.D., Hudnut, K.W., Briggs, R.W., Koehler, R.D. and Jean, P.** (2010) Seismic hazard of the Enriquillo-Plantain fault in Haiti inferred from palaeoseismology. *Nat. Geo.*, **3**, 789–793.
- Prescott, J.R. and Hutton, J.T.** (1994) Cosmic ray contributions to dose rates for luminescence and ESR dating: large depths and long-term time variations. *Radiat. Meas.*, **23**, 497–500.
- Preti, M.** (1999) The Holocene transgression and the land-sea interaction south of the Po delta. *Giorn. Geol.*, **61**, 143–159.
- Regione Emilia-Romagna and ENI-AGIP** (1998) *Riserve idriche sotterranee della Regione Emilia-Romagna*. S.EL.CA, Florence, Italy.
- Regione Lombardia and ENI-Divisione AGIP** (2002) *Geologia degli acquiferi padani della Regione Lombardia*. S.EL.CA, Florence, Italy.
- Reimer, P.J., Bard, E., Bayliss, A., Beck, J.W., Blackwell, P.G., Bronk Ramsey, C., Buck, C.E., Cheng, H., Edwards, R.L., Friedrich, M., Grootes, P.M., Guilderson, T.P., Hafflidason, H., Hajdas, I., Hatté, C., Heaton, T.J., Hoffmann, D.L., Hogg, A.G., Hughen, K.A., Kaiser, K.F., Kromer, B., Manning, S.W., Niu, M., Reimer, R.W., Richards, D.A., Scott, E.A., Southon, J.R., Staff, R.A., Turney, C.S.M. and Van Der Plicht, J.** (2013) IntCal13 and Marine13 radiocarbon age calibration curves, 0–50,000 years cal BP. *Radiocarbon*, **55**, 1869–1887.
- Ricci Lucchi, F.** (1986) Oligocene to Recent foreland basins of northern Apennines. In: *Foreland Basins* (Eds Allen, P. and Homewood, P.), *IAS Special Publication*, **8**, 105–139.
- Rossetti, D.F., Cohen, M.C.L., Bertani, T.C., Hayakawa, E.H., Paz, J.D.S., Castro, D.F. and Friaes, Y.** (2014) Late Quaternary fluvial terrace evolution in the main southern Amazonian tributary. *Catena*, **116**, 19–37.
- Rossi, V.** (2009) Ostracod assemblages from Holocene subsurface deposits of modern Po Delta: a palaeoenvironmental proxy record. *Boll. Soc. Paleontol. It.*, **48**, 95–103.
- Rossi, V. and Vaiani, S.C.** (2008) Benthic foraminiferal evidence of sediment supply changes and fluvial drainage reorganization in Holocene deposits of the Po Delta. *Mar. Micropaleontol.*, **69**, 106–118.
- Rovida, A., Locati, M., Camassi, R., Lolli, B. and Gasperini, P.** (2019) Italian Parametric Earthquake Catalogue (CPTI15), version 2.0. Istituto Nazionale di Geofisica e Vulcanologia (INGV). <https://doi.org/10.13127/CPTI/CPTI15.2>
- Royden, L., Patacca, E. and Scandone, P.** (1987) Segmentation and configuration of subducted lithosphere in Italy: an important control on thrust-belt and foredeep-basin evolution. *Geology*, **15**, 714–717.
- Salel, T., Bruneton, H. and Lefèvre, D.** (2016) Ostracods and environmental variability in lagoons and deltas along the north-western Mediterranean coast (Gulf of Lions, France and Ebro delta, Spain). *Rev. Micropaléont.*, **59**, 425–444.
- Scarponi, D., Kaufman, D., Amorosi, A. and Kowalewski, M.** (2013) Sequence stratigraphy and the resolution of the fossil record. *Geology*, **41**, 239–242.
- Scarponi, D., Azzarone, M., Kusnerik, K., Amorosi, A., Bohacs, K.M., Drexler, T.M. and Kowalewski, M.** (2017) Systematic vertical and lateral changes in quality and time resolution of the macrofossil record: Insights from Holocene transgressive deposits, Po coastal plain, Italy. *Mar. Petrol. Geol.*, **87**, 128–136.
- Schieber, J.** (2016) Mud re-distribution in epicontinental basins—Exploring likely processes. *Mar. Petrol. Geol.*, **71**, 119–133.
- Scrocca, D., Carminati, E., Doglioni, C. and Marcantoni, D.** (2007) Slab retreat and active shortening along the central-northern Apennines. In: *Thrust Belts and Foreland Basins. From Fold Kinematics to Hydrocarbon Systems* (Eds Lacombe, O., Lavé, J., Roure, F. and Vergés, J.), pp. 471–487. Springer Verlag, Berlin.
- Sinha, R., Tandon, S.K., Gibling, M.R., Bhattacharjee, P.S. and Dasgupta, A.S.** (2005) Late Quaternary geology and

- alluvial stratigraphy of the Ganga basin. *Himalayan Geol.*, **26**, 223–240.
- Soil Survey Staff** (1999) *Soil taxonomy. A basic system of soil classification for making and interpreting soil surveys, Agricultural Handbook* (second edition), no. 436. Natural Resources Conservation Service, USDA, Washington DC, 886 p.
- Stefani, M., Minarelli, L., Fontana, A. and Hajdas, I.** (2018) Regional deformation of late Quaternary fluvial sediments in the Apennines foreland basin (Emilia, Italy). *Int. J. Earth Sci.*, **107**, 2433–2447.
- Tamura, T., Murakami, F. and Watanabe, K.** (2010) Holocene beach deposits for assessing coastal uplift of the northeastern Boso Peninsula, Pacific coast of Japan. *Quatern. Res.*, **74**, 227–234.
- Toscani, G., Burrato, P., Di Bucci, D., Seno, S. and Valensise, G.** (2009) Plio-Quaternary tectonic evolution of the northern Apennines thrust fronts (Bologna–Ferrara section, Italy): seismotectonic implications. *Italian J. Geosci.*, **128**, 605–613.
- Vail, P.R., Mitchum, R.M. Jr., and Thompson, S. III** (1997) Seismic stratigraphy and global changes of sea level, part 4: Global cycles of relative changes of sea level. In: *Seismic Stratigraphy – Applications to Hydrocarbon Exploration* (Ed Payton, C.E.), *Am. Ass. Petr. Geol. Memoir*, **26**, 83–97.
- Van der Zwaan, G.J. and Jorissen, F.J.** (1991) Biofacial patterns in river-induced shelf anoxia. In: *Modern and Ancient Continental Shelf Anoxia* (Eds Tyson, R.V. and Pearson, T.H.), *Geol. Soc. Special Publication*, **58**, 65–82.
- Whitney, B.B. and Hengesh, J.V.** (2015) Geomorphological evidence for late Quaternary tectonic deformation of the Cape Region, coastal west Central Australia. *Geomorphology*, **241**, 160–174.

Manuscript received 21 April 2020; revision 30 June 2020; revision accepted 2 July 2020

Supporting Information

Additional information may be found in the online version of this article:

Table S1. List of radiocarbon dated samples of Figs 4 and 5. KGM: samples dated at KIGAM Laboratory, South Korea.

Table S2. List of historical and instrumental earthquakes reported in Fig. 1.